









# Next generation ferroelectric materials for semiconductor process integration and their applications

Cite as: J. Appl. Phys. **129**, 100901 (2021); doi: [10.1063/5.0037617](https://doi.org/10.1063/5.0037617)

Submitted: 14 November 2020 · Accepted: 10 February 2021 ·

Published Online: 11 March 2021



T. Mikolajick,<sup>1,2,a)</sup>  S. Slesazeck,<sup>1</sup>  H. Mulaosmanovic,<sup>1</sup>  M. H. Park,<sup>3</sup>  S. Fichtner,<sup>4</sup>  P. D. Lomenzo,<sup>1</sup>   
M. Hoffmann,<sup>1</sup>  and U. Schroeder<sup>1</sup> 

## AFFILIATIONS

<sup>1</sup>NaMLab gGmbH, Noethnitzer Str. 64, D-01187 Dresden, Germany

<sup>2</sup>Institute of Semiconductors and Microsystems (IHM), TU Dresden, D-01062 Dresden, Germany

<sup>3</sup>School of Materials Science and Engineering, Pusan National University, 2 Busandaehak-ro 63beon-gil, Geumjeong-gu, Busan 46241, Republic of Korea

<sup>4</sup>Materials and Processes for Micro/Nanosystem Technologies, University of Kiel, Institute for Material Science, Kaiserstr. 2, 24143 Kiel, Germany

<sup>a)</sup>Author to whom correspondence should be addressed: [Thomas.Mikolajick@namlab.com](mailto:Thomas.Mikolajick@namlab.com)

## ABSTRACT

Ferroelectrics are a class of materials that possess a variety of interactions between electrical, mechanical, and thermal properties that have enabled a wealth of functionalities. To realize integrated systems, the integration of these functionalities into semiconductor processes is necessary. To this end, the complexity of well-known ferroelectric materials, e.g., the perovskite class, causes severe issues that limit its applications in integrated systems. The discovery of ferroelectricity in hafnium oxide-based materials brought a renewed interest into this field during the last decade. Very recently, ferroelectricity was also verified in aluminum scandium nitride extending the potential of seeing a wealth of ferroelectric functions in integrated electronics in the future. This paper discusses the prospects of both material systems in various applications.

© 2021 Author(s). All article content, except where otherwise noted, is licensed under a Creative Commons Attribution (CC BY) license (<http://creativecommons.org/licenses/by/4.0/>). <https://doi.org/10.1063/5.0037617>

## I. INTRODUCTION

A ferroelectric (FE) material has two stable polarization states that can be switched from one state into another state by applying an electric field.<sup>1,2</sup> To qualify as a ferroelectric, a material, therefore, needs to have a stable polarization at zero applied field referred to as remanent polarization. Since such ferroelectric polarization is temperature dependent, all ferroelectric materials are also pyroelectric. Moreover, the switching dipoles give rise to a field dependent volume change of the material and, therefore, all ferroelectrics and pyroelectrics are piezoelectric.<sup>3</sup> As a result, ferroelectric materials have a plurality of interesting properties that show a dependence on the applied electric field, temperature, strain, and other parameters. Therefore, they are useful in a wealth of applications including capacitors, memory cells, sensors, actuators, energy storage, and more.<sup>4,5</sup> When it comes to the usage of ferroelectrics in integrated

circuits, the defining property of the ferroelectric, namely, switchable polarization, is the most important property since it can be used for information storage.<sup>5,211,214,215</sup> Here, the field driven switching mechanism, together with the fact that the polarization state will be retained for long times, makes the material an ideal choice to realize nonvolatile memories with low write power.

To realize ferroelectricity in a crystal, the crystal necessarily needs to have a non-centrosymmetric structure together with the ability to switch the position of one or several ions in the lattice between two stable states. This makes ferroelectricity a rare material property that historically could only be observed in quite complex crystal structures involving three or more elements like perovskites. Such materials are difficult to integrate into a semiconductor manufacturing process that has strong requirements with respect to thermal budget, exposure to forming gas anneals, and tight control

of the elements used within the production line. As a result, ferroelectrics integrated into semiconductor processes had limited market success so far. In 2011, it was reported for the first time that in doped hafnium oxide ( $\text{HfO}_2$ ), ferroelectricity could be achieved.<sup>6</sup> This discovery changed the prospects of integrating ferroelectrics into complementary metal–oxide–semiconductor (CMOS) processes since hafnium oxide is a standard material used even in the front end of CMOS processes since 2007.<sup>7</sup> More recently, the piezoelectricity available in AlN could be turned into a switchable ferroelectricity in AlScN.<sup>8</sup> This material would be ideally suited for the integration with GaN technology, but it also promises options for CMOS back end of line integration. Finally, the efforts of making 2D materials usable in electron devices also yielded very interesting ferroelectrics.<sup>9,10</sup> The following article will deal with hafnium oxide-based ferroelectrics as well as AlScN based ferroelectrics since these materials are closest to the real application and, therefore, are very promising to enter commercial semiconductor processes in the next five to ten years.

## II. HISTORY OF FERROELECTRIC MATERIALS AND DEVICES

Recently, the 100th anniversary for the discovery of ferroelectricity in Rochelle salts was celebrated.<sup>11,12</sup> While the interesting properties immediately spurred further research that brought up additional systems like potassium-dihydrogen phosphate, or KDP,<sup>13</sup> these material systems were too sensitive and water-soluble for practical applications. The discovery of ferroelectricity in barium titanate  $\text{BaTiO}_3$  (BTO)<sup>14–16</sup> paved the way for applications in sensors and capacitors. Already in the 1950s, Buck proposed the usage of ferroelectrics for memory applications,<sup>17</sup> and this proposal inspired additional research activities.<sup>18,19</sup> These did not result in products appearing on the market, and integrated circuit technology, as we know it today, was not yet available in those days. Nevertheless, those early devices that contained hundreds of memory cells on a single BTO substrate can be considered the first demonstration of an integrated memory devices.

On the material side, the lead-zirconium titanate  $\text{Pb}[\text{Zr}_x\text{Ti}_{1-x}]\text{O}_3$  (PZT) system<sup>20,21</sup> brought another big step in the 1950s. Like BTO, PZT has a perovskite structure. However, the mixture of Zr and Ti based oxides brings additional flexibility and particularly at the morphotropic phase boundary between the tetragonal and rhombohedral ferroelectric phases possesses excellent ferroelectric properties. In the second half of the 1950s, the concept of a ferroelectric field-effect transistor (FeFET) was proposed for the first time.<sup>22</sup> But it took a very long time until such a device would produce useful characteristics including nonvolatile retention.<sup>23</sup> While basic research on those and other ferroelectric memories continued, the development of integrated circuit processes finally enabled the realization of a ferroelectric memory that could fulfill all of the requirements to be commercialized in the early 1990s.<sup>24</sup> Besides using PZT instead of BTO, the main difference compared to the early attempts from the 1950s was that a select transistor was added to the memory cell to result in a similar cell structure that is known from dynamic random access memories (DRAMs). The select transistor made it possible to eliminate problems from half selects of other bitlines and wordlines. Nevertheless, PZT suffered

from fatigue, which is the degradation of the switchable polarization with increasing read and write cycles.

Layered perovskites that have oxide interlayers between perovskite layers like strontium bismuth tantalate  $\text{Sr}_2\text{Bi}_2\text{TaO}_9$  (SBT) were introduced in the 1990s as a solution to fatigue.<sup>25</sup> However, the even more complex crystal structure made the integration of the layered perovskites into semiconductor fabrication processes even more troublesome than it was for PZT. Therefore, the commercial success was limited since around the same time, fatigue in PZT was found to be greatly reduced by using oxide electrodes like  $\text{IrO}_2$ ,  $\text{RuO}_2$ , and related materials.<sup>26</sup> Even after solving the fatigue issue in PZT, the required crystallization, problematic inclusion of lead, and the weakly bound oxygen make perovskites and layered perovskites still very difficult to integrate into CMOS processes.<sup>27</sup> As a result, the most advanced technology is in the 130 nm node<sup>28</sup> and the three-dimensional integration issue could not be solved up to now.<sup>29</sup> In the mid-2000s, the first demonstration of the nonvolatile operation of a FeFET based on SBT was finally achieved.<sup>30</sup> In the same time period, a concept based on the switchable tunneling current through a very thin ferroelectric that was first proposed by Esaki *et al.* back in 1971<sup>31</sup> was finally realized<sup>32</sup> adding ferroelectric tunnel junctions (FTJs) as a third option to the portfolio of ferroelectric memory devices. However, these devices need high quality epitaxial ferroelectrics.<sup>33</sup> This approach is extremely unlikely to be integrated into a CMOS process. With the known processes for epitaxial growth of such layers and the required lattice matched electrodes, epitaxial growth directly on a CMOS compatible substrate cannot be achieved. An interesting alternative approach for integrating such complex oxide films is to grow the epitaxial films on a different substrate and transfer them to the CMOS wafer,<sup>34,35</sup> but this technique is still in the basic research phase and many years of research will be required to see if this could be a viable path toward CMOS integration. The field, therefore, seems to be stuck in a situation where extremely promising memory properties were demonstrated for three fundamentally different device types, but the integration into state-of-the-art CMOS processes was hindered by the integration issues due to the rather complex materials.

The first report of ferroelectricity in silicon doped hafnium oxide in 2011<sup>6</sup> changed that picture and immediately resulted in the realization of a FeFET with very promising properties.<sup>36</sup> The stabilization of ferroelectricity by several other dopants<sup>37</sup> and the demonstration of three-dimensional structures for capacitor based ferroelectric random access memory (FeRAM),<sup>38</sup> as well as the demonstration of integrated FeRAM devices<sup>39</sup> and FTJs,<sup>40,41</sup> show that this material system immediately brought new life into the field of ferroelectric devices. Besides realizing memories, ferroelectric hafnium oxide is the only material system that could possibly be used when realizing a new type of steep slope device proposed in 2008 under the term negative capacitance field-effect transistor (NCFET)<sup>42</sup> that is still controversially discussed in the community<sup>43</sup> and requires much more basic understanding to verify its potentials and limitations.<sup>44</sup> Finally, in 2019, another interesting new material AlScN was added to the list of new ferroelectrics.<sup>8</sup> While in hafnium oxide-based ferroelectrics, a phase that is normally not stable in bulk materials is stabilized in thin films, in the AlScN system, a well-known piezoelectric material was made ferroelectric. Again, a ferroelectric material that is much more

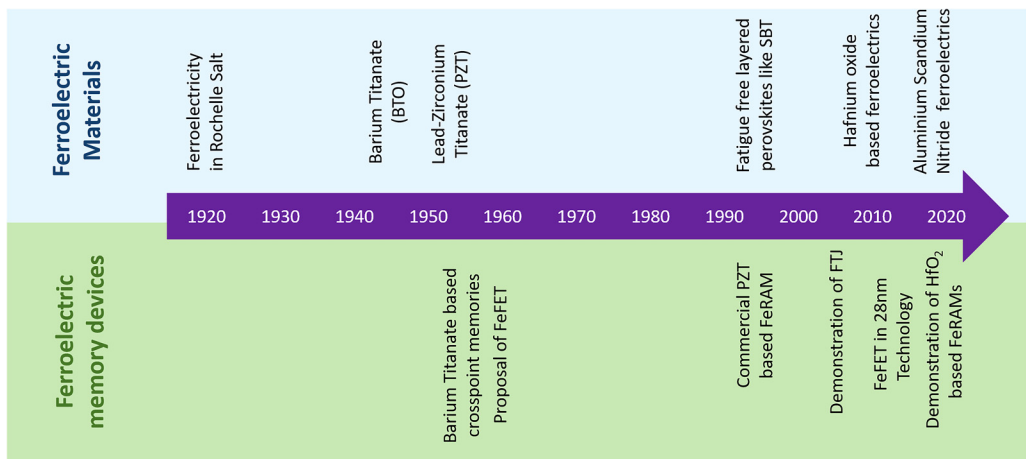


FIG. 1. Timeline of ferroelectric materials and ferroelectric semiconductor devices.

compatible to semiconductor processing is added. The timeline of ferroelectric materials and ferroelectric semiconductor devices is illustrated in Fig. 1.

III. FERROELECTRIC MATERIALS

A. Traditional ferroelectric materials

Ferroelectricity can be shown in various types of materials with non-centrosymmetric crystalline structures, and they can be categorized into various groups according to their mechanism behind ferroelectricity. In this section, however, only those materials, which have been seriously considered for being utilized in semiconductor industry, are focused on. The first and second

discovered ferroelectric materials were Rochelle salt<sup>11</sup> and KH<sub>2</sub>PO<sub>4</sub><sup>13</sup> in 1920 and 1935, respectively. After the discovery of ferroelectricity in perovskite structure BaTiO<sub>3</sub>, the ferroelectric materials attracted significant interest from the 1940s on Ref. 16. Since then, the perovskite structure ferroelectrics have been the largest group among various material groups to date.

Figure 2 and Table I summarize the crystalline structures and material properties of several relevant conventional ferroelectrics: Pb(Zr,Ti)O<sub>3</sub> (PZT), SrBi<sub>2</sub>Ta<sub>2</sub>O<sub>9</sub> (SBT), and BiFeO<sub>3</sub> (BFO). PZT is the most intensively studied ferroelectric material for various applications including FeRAMs, actuators, and sensors based on its strong ferroelectricity and piezoelectricity. Its remanent polarization (P<sub>r</sub>) is generally 10–40 μC/cm<sup>2</sup> in thin films and can be even higher

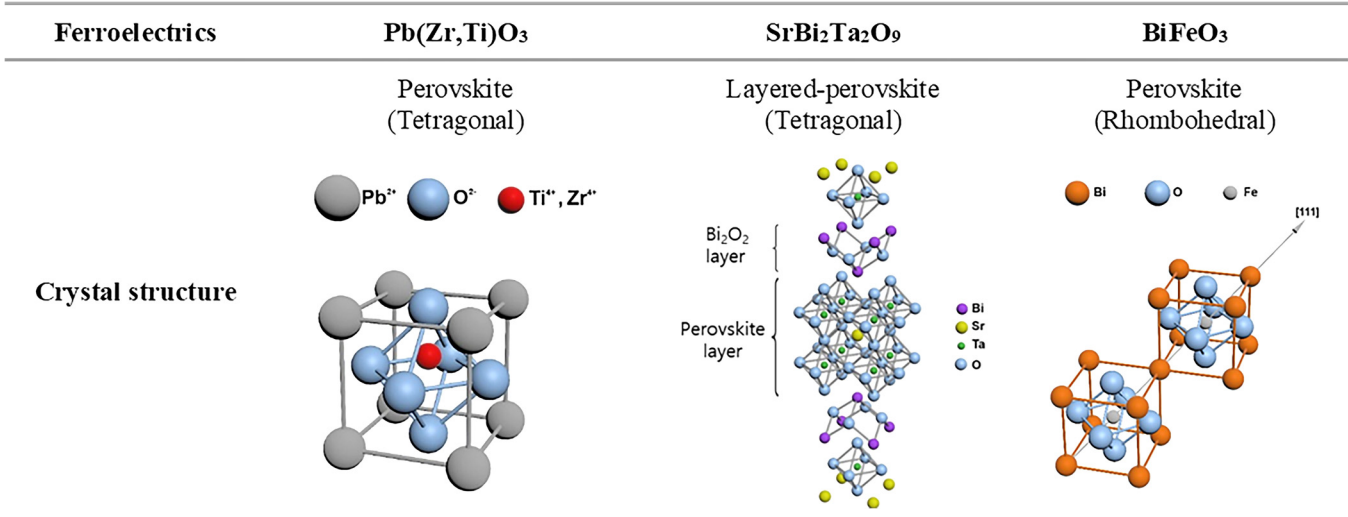


FIG. 2. Conventional ferroelectric materials: Pb(Zr,Ti)O<sub>3</sub>, SrBi<sub>2</sub>Ta<sub>2</sub>O<sub>9</sub>, and BiFeO<sub>3</sub>.

**TABLE I.** Comparison of ferroelectric materials PZT, SBT, BFO, doped HfO<sub>2</sub>, and Al<sub>x</sub>Sc<sub>1-x</sub>N.

Ferroelectrics	Pb(Zr,Ti)O <sub>3</sub> <sup>99,100</sup>	SrBi <sub>2</sub> Ta <sub>2</sub> O <sub>9</sub> <sup>25</sup>	BiFeO <sub>3</sub> <sup>46,47</sup>	Doped HfO <sub>2</sub> Hf <sub>x</sub> Zr <sub>1-x</sub> O <sub>2</sub> <sup>101,102</sup>	Al <sub>x</sub> Sc <sub>1-x</sub> N <sup>8</sup>
P <sub>r</sub> (μC/cm <sup>2</sup> )	10–40	5–10	90–95 (along [111])	10–40	80–110
E <sub>c</sub> (kV/cm)	50–70	30–50	100–1500	800–2000	2000–5000
ε <sub>0</sub>	~400	~200	~50	~30	~25
Endurance (cycles)	>1 × 10 <sup>15</sup> on oxide electrode	Good on Pt electrode	Good on oxide electrode	>1 × 10 <sup>11</sup> on TiN	>1 × 10 <sup>5a</sup>
Min. physical thickness (nm)	50			<5	<50 <sup>a</sup>
Crystallization temperature (°C)	Low	High	Low	400–800	300–400
Curie temperature (°C)	~400	~400	~700	0–500	>600

<sup>a</sup>Early results, improvements expected.

than 70 μC/cm<sup>2</sup>, so in FeRAM capacitors of nonvolatile memory cell, a large quantity of charges can be stored. When PZT was first adopted to FeRAMs, the limited number of endurable cycles with significant fatigue was a critical issue using Pt electrodes,<sup>45</sup> so other oxide electrodes such as IrO<sub>2</sub> were introduced to achieve an endurance that was sufficient for practical FeRAMs. SBT attracted intensive focus for FeRAM application, since it could exhibit fatigue-free performance on Pt electrodes.<sup>25</sup> The remanent polarization P<sub>r</sub> of SBT thin films is 5–10 μC/cm<sup>2</sup>, which is smaller compared to that of PZT, but it is sufficient to control the Si channel conductivity in FeFETs and for storing charges in FeRAM cells. As a result, SBT was intensively studied for FeRAMs and FeFETs with high reliability despite its complexity in chemical composition and crystalline structure. BFO is based on a rhombohedral perovskite structure, and it could exhibit polarization as high as ~100 μC/cm<sup>2</sup>.<sup>46,47</sup> With such high polarization, BFO has attracted increasing interest for various applications. However, as insulating ferroelectric ceramics for memory technology, BFO has the intrinsically critical issue of a small bandgap (2.0–2.5 eV). Instead, BFO can exhibit ferromagnetic properties as well as giant ferroelectric property, which enables applications based on electro-magnetic coupling even at room temperature. Moreover, with a bandgap significantly smaller than those of PZT or SBT, BFO was suggested to be promising for photovoltaic applications.<sup>48</sup>

## B. Hafnium and zirconium based ferroelectrics

The ferroelectricity in Si-doped HfO<sub>2</sub> was first reported in 2011 by Börscke and co-workers.<sup>36,49</sup> Different from conventional ferroelectric materials that suffer from the serious degradation of ferroelectricity in ultra-thin films, a robust ferroelectricity with P<sub>r</sub> higher than 15 μC/cm<sup>2</sup> could be achieved with 10 nm film thickness.<sup>36</sup> This pioneering work was followed by numerous reports on ferroelectricity in HfO<sub>2</sub> or ZrO<sub>2</sub> induced by various dopants and deposition techniques.<sup>50–56</sup> Figure 3(a) shows several polymorphs of HfO<sub>2</sub> and ZrO<sub>2</sub> frequently observed in thin films, and the crystallographic origin of the ferroelectricity is the formation of the Pca2<sub>1</sub> orthorhombic phase, as demonstrated by Sang *et al.*<sup>57</sup> using convergent beam electron beam diffraction. Generally, nanoscale competition between different crystalline phases can be observed in doped HfO<sub>2</sub> or ZrO<sub>2</sub> thin films, which is affected by various factors including doping, thickness, impurities, temperature, and even electric field cycling. Such

complicated nanoscale polymorphism can be attributed to the metastability of the ferroelectric orthorhombic phase.<sup>58–63</sup>

Figures 3(b)–3(d) show the effect of doping on x-ray diffraction (XRD) pattern, aspect ratio, and relative phase fraction, respectively.<sup>64</sup> As can be seen in Fig. 3(b), the dominant crystalline phase changes from monoclinic to orthorhombic to tetragonal/cubic phase with increasing doping concentration, and there exist a specific doping concentration range dependent on dopant species where strong ferroelectricity with high orthorhombic phase fraction can be achieved. The ideal aspect ratios, which are relative ratios of the largest lattice parameter to the shorter ones, expected for the orthorhombic and tetragonal phase are ~1.03–1.04 and 1.01–1.02, respectively.<sup>65</sup> Thus, a high aspect ratio is one important sign of ferroelectricity in doped HfO<sub>2</sub> or ZrO<sub>2</sub>. As reported by Park *et al.*,<sup>65</sup> the Rietveld refinement can be utilized to quantitatively analyze the relative fractions of different crystalline phases. Figure 3(d) shows the Rietveld refinement result of La-doped HfO<sub>2</sub> thin films with various doping concentrations, which is consistent with changes in ferroelectric properties. As shown in Fig. 3(e), the unit cell size of the ferroelectric orthorhombic phase increases with increasing dopant radius.

The film thickness is another factor that critically affects the ferroelectricity in doped HfO<sub>2</sub> or ZrO<sub>2</sub> films. Figure 3(f) shows the changes in the P<sub>r</sub> value of HfO<sub>2</sub> films doped with various dopants as functions of the film thickness.<sup>64</sup> Generally, the orthorhombic phase fraction as well as P<sub>r</sub> decrease with increasing film thickness and, therefore, with decreasing surface-to-volume ratio. As suggested by Materlik *et al.*,<sup>58</sup> the polymorphism in fluorite-structure ferroelectrics is strongly influenced by a surface energy effect. The effect of the thickness on the coercive field (E<sub>c</sub>) in fluorite-structure ferroelectrics is different from normal ferroelectrics as shown in Fig. 3(g).<sup>66</sup> It is generally known that E<sub>c</sub> of ferroelectrics is proportional to d<sup>-3/2</sup>, but the thickness dependence of polycrystalline Hf<sub>0.5</sub>Zr<sub>0.5</sub>O<sub>2</sub> or epitaxial Y:HfO<sub>2</sub> is much weaker than expectation from the Kay–Dunn model.<sup>67</sup> The authors have shown that small crystallites shift independent of their environment and even micrometer thick films consist of these nanometer sized crystallites, which determine the switching kinetics. A schematic phase diagram for HfO<sub>2</sub>–ZrO<sub>2</sub> solid solution with various doping concentrations and thicknesses can be seen in Fig. 3(h).<sup>68</sup> The monoclinic phase fraction is higher for thicker and Hf-rich films, while the tetragonal phase fraction is higher for thinner and Zr-rich films.

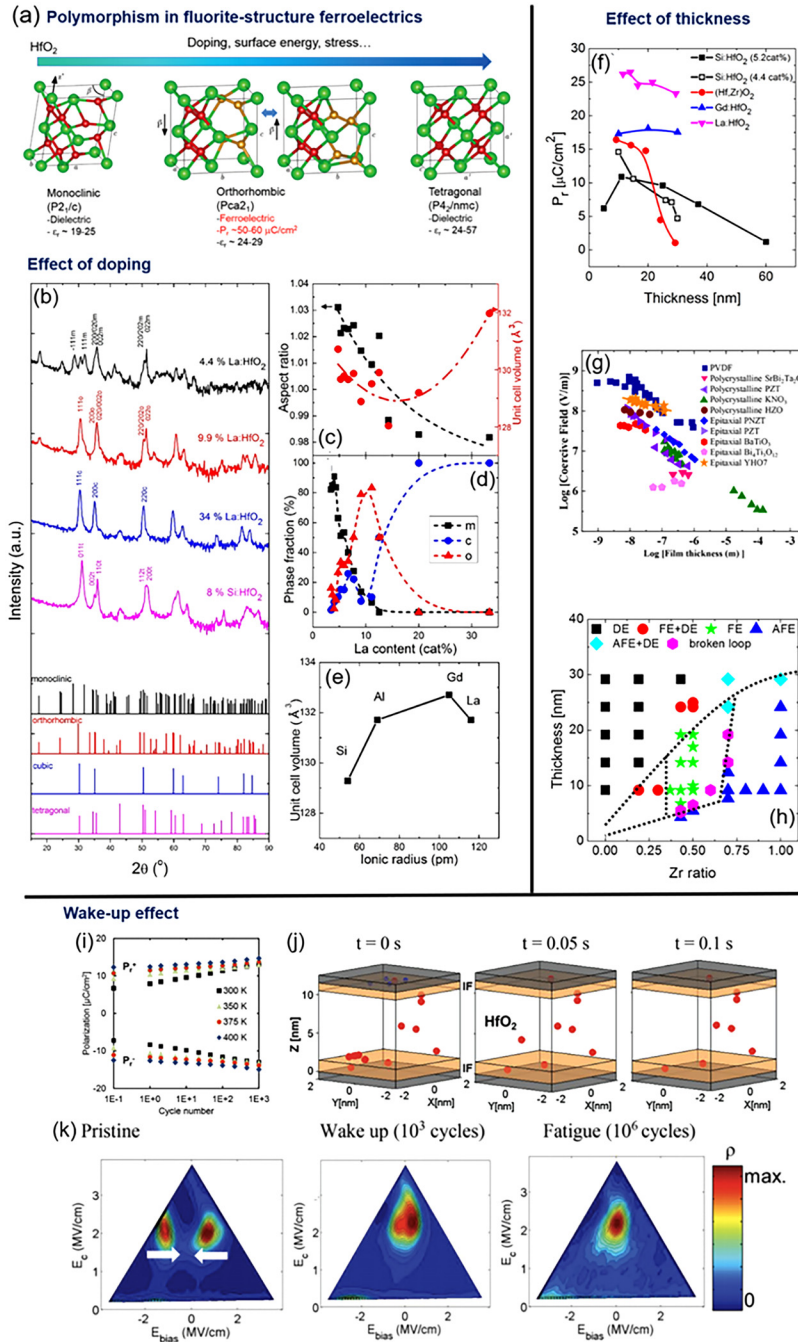


**FIG. 3.** (a) General trend in polymorphism in ferroelectric doped HfO<sub>2</sub> thin films. (b) X-ray diffraction patterns of La:HfO<sub>2</sub> and Si:HfO<sub>2</sub> thin films. The changes in (c) aspect ratio/unit cell volume and (d) relative phase fraction in La:HfO<sub>2</sub> as functions of La content. (e) The unit cell volume of the ferroelectric orthorhombic phase as a function of ionic radius of dopants. (a) Reproduced with permission from Park *et al.*, J. Mater. Chem. C 5(19), 4677–4690 (2017). Copyright 2017 Royal Society of Chemistry. (b)–(e) From Part *et al.*, “Dopants in atomic layer deposited HfO<sub>2</sub> thin films,” in *Ferroelectricity in Doped Hafnium Oxide: Materials, Properties and Devices*. Copyright 2020 Elsevier. Reprinted with permission from Elsevier. (f) From Park *et al.*, “Effect of surface/interface energy and stress on the ferroelectric properties,” in *Ferroelectricity in Doped Hafnium Oxide: Materials, Properties and Devices*. Copyright 2020 Elsevier. Reprinted with permission from Elsevier. (g) Reproduced with permission from Mimura *et al.*, Appl. Phys. Lett. 113 (10), 102901 (2018). Copyright 2018 AIP Publishing LLC. (h) Reproduced with permission Part *et al.*, Nanoscale 9, 9973–9986 (2017). Copyright 2017 Royal Society of Chemistry. (i)–(k) Reproduced with permission from Pešić *et al.*, Adv. Funct. Mater. 26(25), 4601–4612 (2016). Copyright 2018 John Wiley and Sons.



Strong ferroelectricity can be observed at a Zr content of 50% and a thickness range of 7–20 nm, and a qualitatively similar trend can be observed in  $\text{HfO}_2$  films doped with other dopants.<sup>68</sup>

The ferroelectricity in fluorite-structure ferroelectrics is also dynamically affected by the electric field cycling. The phenomenon describing the increase of the remanent polarization for low cycle counts is called the “wake-up effect”<sup>69–72</sup> while the phenomenon that leads to the reduction in  $P_r$  at high cycle count is called the “fatigue effect.” Figure 3(i) shows the field-cycling-number-dependent evolution of the  $P_r$  values in  $\text{Gd:HfO}_2$  thin films at various measurement temperatures, as reported by Pešić and co-workers.<sup>70</sup> As shown in Fig. 3(j), the changes in  $P_r$  could be a simulated redistribution of oxygen vacancies, which are expected to result in variations of the local field distribution and/or resulting local phase transitions. From the first-order reversal curve (FORC) measurement shown in Fig. 3(k), it can be identified that the inhomogeneous positive and negative internal bias in the pristine state almost disappeared after the wake-up field cycling. These results suggest that the oxygen vacancies concentrated at the interfacial region are more homogeneously redistributed.<sup>70</sup> Additionally, non-polar interfacial layers could degrade.<sup>70</sup> During the fatigue stage after the wake-up process, the oxygen vacancy concentration is expected to increase similar to what is observed in conventional ferroelectric materials. The cycling endurance is typically limited by fatigue with  $P_r$  decrease or hard breakdown resulting from the permanent conducting path formation due to the accumulation of oxygen vacancies.<sup>70</sup> Moreover, a phase transition could be observed in transmission electron microscopy (TEM) studies during the wake-up process,<sup>72</sup> but the amount of phase transition could not be determined from synchrotron-based x-ray diffraction (XRD) studies.

### C. Ferroelectricity in wurtzite aluminum scandium nitride

Unlike in  $\text{HfO}_2$  and  $\text{ZrO}_2$  based ferroelectrics, the occurrence of ferroelectricity in  $\text{AlScN}$  does not originate in the stabilization of

additional pyroelectric phases through doping or strain—but rather through the destabilization of its parent, already polar wurtzite phase (space group  $P6_3mc$ ) by forming solid solutions with binary nitrides that exhibit a tendency for fivefold coordination<sup>8,75,76</sup>—i.e., space group  $P6_3/mmc$  [see Figs. 4(a) and 4(c)]. Thus, and through the application of tensile stress on the wurtzite basal plane, the coercive field of  $\text{AlScN}$  can become smaller than the dielectric breakdown strength. As a result, the material becomes ferroelectric. In other words, the addition of Sc flattens the overall energy landscape of the wurtzite structure, leading to a reduced energy barrier between the two polarization states of the material, N-polar and metal-polar (M-polar) [see Figs. 4(a) and 4(c)]. Structurally, this energy barrier can be associated with  $P6_3/mmc$  (layered hexagonal structure), which is the closest higher symmetry relative of the wurtzite structure. Both structures only differ in their internal parameter  $u$ , defined as the length of the  $c$  axis parallel metal–nitrogen bond relative to the lattice parameter  $c$ . For the wurtzite structure,  $u < 0.5$ , while for  $P6_3/mmc$ ,  $u = 0.5$ —which implies that metal and nitrogen atoms share a common plane in the latter. Thus, the energetic approach between wurtzite and  $P6_3/mmc$  also lowers the energy that is required for metal and nitrogen planes to switch their positions along the  $c$  axis of the material, i.e., the structural change that is required to alternate between the polarization states of the wurtzite structure. This mechanism in turn lowers the coercive field, which roughly speaking is the electric field required to switch from  $P6_3mc$  to  $P6_3/mmc$ , until and beyond the point where  $\text{AlScN}$  becomes ferroelectric. A qualitative illustration of the evolution of the double well potential under the addition of Sc is given in Fig. 4(c). This mechanism should in principle be extendable to other wurtzite semiconductors such as  $\text{GaN}$ <sup>75</sup> or  $\text{ZnO}$ <sup>77</sup>—provided that they can be synthesized with sufficient breakdown strength and suitable compounds can be identified for solid solution formation.

The interest in  $\text{AlScN}$  and related wurtzite solid solutions can be traced back to DFT calculations by Takeuchi<sup>78</sup> as well as Farrer and Bellaiche<sup>79</sup> who in 2002 motivated the (meta-)stability of a

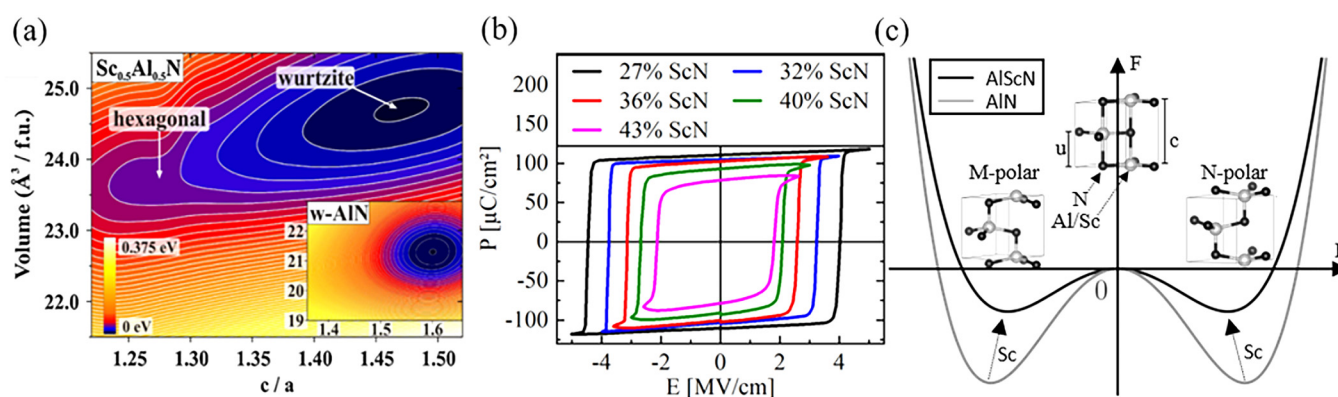


**FIG. 4.** (a) DFT simulated energy landscape of  $\text{Al}_{0.5}\text{Sc}_{0.5}\text{N}$  compared to pure  $\text{AlN}$ .<sup>76</sup> (b) P–E loops of  $\text{AlScN}$  films with Sc contents between 27% and 43% ScN.<sup>8</sup> (c) Qualitative evolution of the wurtzite-inherent double well potential under addition of Sc with respective unit cells belonging to the two minima (M-polar and N-polar, wurtzite structure) as well as the intermediate energy barrier (non-polar, layered hexagonal structure). (a) Reprinted with permission from Tasnadi *et al.*, Phys. Rev. Lett. **104**, 137601 (2010). Copyright 2010 American Physical Society. (b) and (c) Reprinted with permission from Fichtner *et al.*, J. Appl. Phys. **125**, 114103 (2019). Copyright 2019 AIP Publishing LLC.

hexagonal ScN phase as well as some of its potential implications on the properties of III-N–ScN solid solutions. In 2009, Akiyama *et al.* experimentally confirmed that the wurtzite structure of sputtered AlScN thin films is stable over wide compositional and temperature ranges—crucially, they could also demonstrate a more than fourfold increase in the longitudinal piezoelectric coefficient compared to pure AlN,<sup>80</sup> when increasing the Sc content. Consequently, their report led to substantial interest in AlScN from the micro-electro-mechanical systems (MEMS) community, where pure AlN was already a well-established material for actuators, sensors, and particularly acoustic resonators. Thanks to this effort, AlScN PVD processes are fully industrialized today and AlScN bulk acoustic wave (BAW) resonators are a crucial part of 4G and 5G kits for mobile communication<sup>81</sup>—which can be of great advantage considering a potential industrialization of ferroelectric AlScN. At the same time, there were already a number of indicators that, in retrospective, hinted at the possibility of ferroelectricity in AlScN through an energetic and structural approach toward  $P6_3/mmc$  (layered hexagonal structure) and consequently a flatter energy landscape between the polarization states of the wurtzite structure [see Fig. 4(a)]. Besides the enhanced piezoelectric coefficients, this included a more than twofold increase in permittivity, decreased stiffness, and a substantial decrease in the lattice parameter ratio  $c/a$ .<sup>80,82–84</sup> Similar trends might herald future ferroelectrics. In spite of this and the theoretical motivation of wurtzite ferroelectrics,<sup>75,77</sup> the effect was not generally anticipated by the community—in part perhaps due to a number of spurious reports on ferroelectric ZnO<sup>85,86</sup> and the breaking of covalent bonds that is required for a change in the wurtzite polarization direction.

Polarization states of the wurtzite unit cell separated by intermediate layered hexagonal structure.<sup>8</sup>

The eventual discovery of ferroelectricity in AlScN<sup>8</sup> created attention through a number of presently almost unique features: Both the spontaneous polarization ( $80\text{--}110\text{ }\mu\text{C}/\text{cm}^2$ ) and the coercive fields ( $1.8\text{--}5\text{ MV}/\text{cm}$ ) reach values that were only sporadically reported in other materials. In addition, both parameters are systematically adjustable by the amount of ScN (typically 20%–43%) and basal plane stress [see Fig. 4(b)]. Next, AlScN is the first readily available nitride ferroelectric and at least its fabrication by PVD allows the combination of post-CMOS compatible deposition temperatures ( $<400\text{ }^\circ\text{C}$ ) with good temperature stability (no loss of net-polarization up to at least  $600\text{ }^\circ\text{C}$ ).

As a material originating from MEMS technology, the application of ferroelectric AlScN to enable, e.g., multi-layer actuators with improved stress-per-voltage output appears comparably straightforward.<sup>87</sup> Still, it may be expected that the majority of application driven research on ferroelectric AlScN will focus on its integration in memory and logic ICs based on their significantly larger market share. This implies the option for substantially lower switching voltages to allow an FeRAM that can be operated from the chip supply voltage in scaled technologies reduced charge leakage while at the same time improving the endurance and developing deposition methods that are more suitable for state-of-the-art technology nodes than PVD. It is safe to assume that the reduction of the switching voltage will be mainly achieved through decreasing the thickness of AlScN films to below 20 nm. Recent results indicate that this approach is indeed feasible with ferroelectricity observed

down to thicknesses that approach 20 nm, resulting in single-digit switching voltages.<sup>88</sup> Similar to  $\text{HfO}_2$  and  $\text{ZrO}_2$  based materials, the coercive fields and the remanent polarization were observed to stay almost constant between several 10 nm and several 100 nm film thickness [see Figs. 5(a) and 5(c)].<sup>88,89</sup> In view of the already large initially reported coercive fields in 400–1000 nm thick films, this new perception removes one of the main risks that had to be initially associated with scaling ferroelectric AlScN. Strict adherence to the Kay–Dunn model would make the necessary reduction of the coercive voltage by thickness scaling impossible.

Next, increasing the ratio between the coercive field and the dielectric breakdown field could prove instrumental for reducing both charge injection and increasing the number of possible switching cycles. Besides conducting more rigorous studies on the ideal film composition in terms of the Al/Sc ratio, processes and material combinations that result in more tensile basal plane stress have to be developed to this end. The thus reduced coercive fields would also bring AlScN to the interval that is employed in  $\text{HfO}_2$ -based FeFETs ( $0.8\text{--}2\text{ MV}/\text{cm}$ ), while coercive fields significantly below  $1\text{ MV}/\text{cm}$  can be currently considered out of scope for wurtzite ferroelectrics.

As in other ferroelectrics, the nature of the conductor/ferroelectric interface can also be expected to play a fundamental role in this matter. The main challenge here will be to identify interfaces that suppresses charge injection and at the same time promote textured growth of AlScN, preferably under tensile film stress. In the context of leakage suppression, it is encouraging that Yasuoka *et al.* were able to demonstrate polarization–electric field (P–E) loops in 79 nm thin AlScN films that were virtually leakage free [Fig. 5(c)]—yet, a comparative study would be of use to understand to which aspect of their experimental details this is related (e.g., measurement frequency, deposition process, Sc content, and so on).<sup>89</sup> In terms of deposition methods, ALD would be preferable from the integration point of view—due to superior conformity, thickness control, substrate size, and homogeneity. While both processes for textured AlN and precursors for Sc exist,<sup>91–94</sup> it remains to be investigated whether the necessary degree of texture and breakdown resistance can indeed be realized at reasonable deposition temperatures, even when employing plasma to support crystallization. In terms of structural quality, MBE and MOCVD processes of AlScN have already progressed further, albeit at the price of higher deposition temperatures.<sup>95,96</sup> Still, ferroelectricity in AlScN films deposited by other means than sputtering is yet to be demonstrated and remains one of the foremost goals.

Since the spontaneous polarization of AlScN is systematically lowered by approaching the non-polar layered hexagonal phase with increasing Sc content, the material also offers novel approaches for polarization engineering in III-N heterostructures<sup>97,98</sup> with the goal to achieve larger sheet charges in 2D electron gases (2DEGs) for high electron mobility transistors (HEMTs). The realization that the polarization of the wurtzite structure is at least one order of magnitude above what was predicted in earlier calculations together with the flexibility that a native III-N based ferroelectric offers in terms of polarization direction can also be expected to lead to new concepts in the field of polar heterostructures with potentially far reaching implications for power and RF electronics.

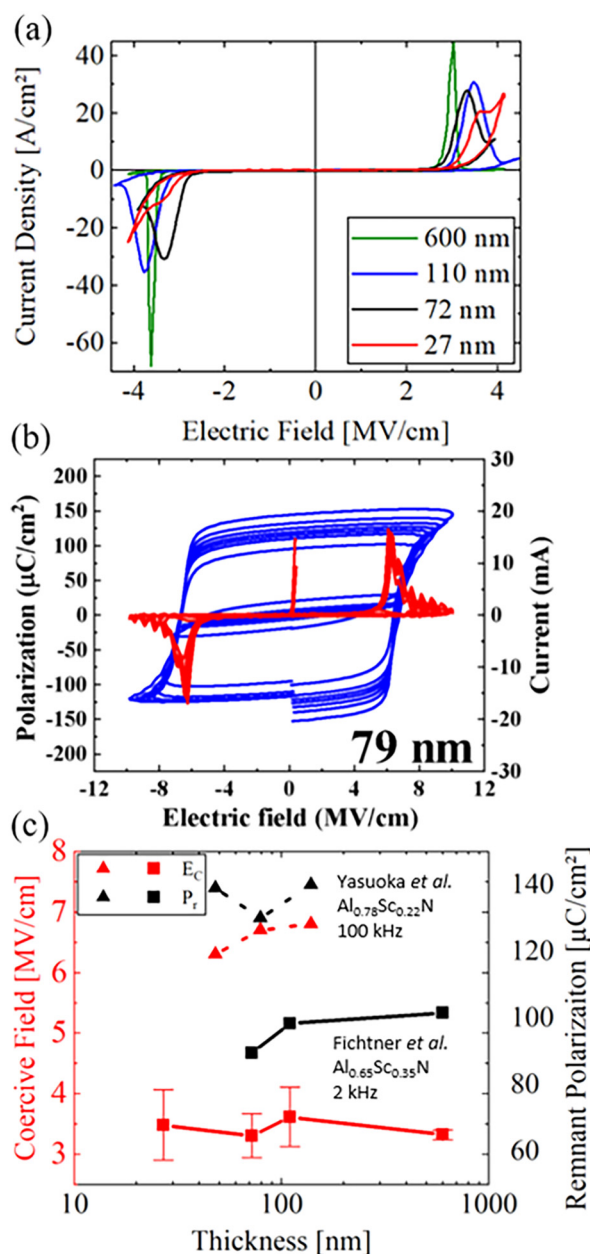


**FIG. 5.** (a) Current vs electric field of  $\text{Al}_{0.65}\text{Sc}_{0.35}\text{N}$  films with varying thickness<sup>84</sup>—as of now, leakage currents increase substantially when reducing film thickness. (b) Virtually leakage free P-E loop and underlying current vs electric field of a 79 nm thick  $\text{Al}_{0.78}\text{Sc}_{0.22}\text{N}$  film.<sup>85</sup> (c) Coercive field and remnant polarization over film thickness of AlScN.<sup>84,85</sup> While a direct comparison between the two available sources is not possible due to different Sc contents and measurement frequency, it can still be concluded that the coercive field does not significantly increase for thinner films. (a) From Fichtner, "Ferroelectricity in AlScN: Switching, imprint and sub-150nm films," in *Proceedings of 2020 IEEE IFCS/ISAF* (IEEE, 2020). Copyright 2020 IEEE. Reprinted with permission from IEEE. (b) Reprinted with permission from Yasuoka et al., *J. Appl. Phys.* **128**, 114103 (2020). Copyright 2020 AIP Publishing LLC.

## D. Material comparison and perspectives

Looking at the overview of the properties for all materials discussed in the text above (Table I),<sup>8,25,46,47,99,102,103,825</sup> remanent polarization values are similar in the range of  $10\text{--}100\text{ }\mu\text{C}/\text{cm}^2$  with  $\text{BiFeO}_3$  and  $\text{Al}_x\text{Sc}_{1-x}\text{N}$  having the highest reported values. In contrast, the coercive field and the dielectric constant can vary by two orders of magnitude. As discussed in the literature, the coercive field according to the Landau theory is expected to be proportional to  $1/\epsilon_r$  in a wide range of dielectric constants.<sup>104</sup> This means that  $E_c$  is a material property, which can only be drastically changed together with the dielectric constant. Both  $\text{HfO}_2$  and AlScN based ferroelectrics have a high coercive field, which results in an improved stability of the polarization but also in higher switching fields. Since  $E_c$  is close to the breakdown field, the cycling endurance of the devices becomes critical. In addition, since under the assumption that non-polarized layers in series with the ferroelectric layer have a similar dielectric constant as the ferroelectric itself, the depolarization field<sup>105</sup> is roughly proportional to  $P_r/\epsilon_r$ . Accordingly, much higher depolarization field values are expected for  $\text{Al}_x\text{Sc}_{1-x}\text{N}$  and  $\text{BiFeO}_3$  for films with the same film thickness [Table I, Fig. 6(a)]. As a result, depolarization will lead to much lower practically achievable polarization values since high polarization values will lead to a fast retention loss. For all materials, the Curie temperature is above  $400^\circ\text{C}$ , which typically enables operation below  $200^\circ\text{C}$ , and low crystallization temperatures are shown for most materials that are important for back-end-of line integration.

Conventional perovskite ferroelectrics are currently used in several devices due to their mature ferroelectric performance and cycling stability.<sup>106</sup> Here, the most critical issue of the materials was limited scalability and CMOS compatibility.<sup>27,29</sup> Moreover, the minimum film thickness achievable with the state-of-the-art fabrication technique is larger than 50 nm. With scaling down of 1T1C FeRAMs, the adoption of three-dimensional capacitors is crucial, but the thickness of ferroelectric film needs to be as small as 1/3 of the feature size. Thus, the film thickness of 50 nm cannot be applied to the state-of-the-art nanoscale semiconductor devices. The coercive field ( $E_c$ ) of PZT and SBT thin films is  $101\text{--}102\text{ kV}/\text{cm}$ , and to achieve 1.0 V memory window (MW) in a FeFET structure, a 50–500 nm film thickness is required. With the down-scaling of FeFET devices, the film thickness of a ferroelectric gate oxide cannot be decreased below 50 nm to achieve sufficient memory window for reliable operation.<sup>107</sup> As a result, the scaling of FeRAMs got limited to the 130 nm technology node and FeFETs using perovskites never made it beyond lab demonstrations.<sup>30</sup> The technology node for commercial FeRAM is about an order of magnitude larger compared to other advanced semiconductor devices, and therefore, the commercial applications of ferroelectric materials in memory devices are limited to niche markets.

The most critical issues for fluorite-structure ferroelectrics are (1) the complicated polymorphism originating from nanoscale competition of different crystalline phases, which becomes an issue for fabricating integrated devices with uniform performance; (2) the limited field cycling endurance originating from the high electric field required for achieving a saturated polarization due to the high  $E_c$  of  $0.8\text{--}2.0\text{ MV}/\text{cm}$ ; (3) the dynamic evolution of electric



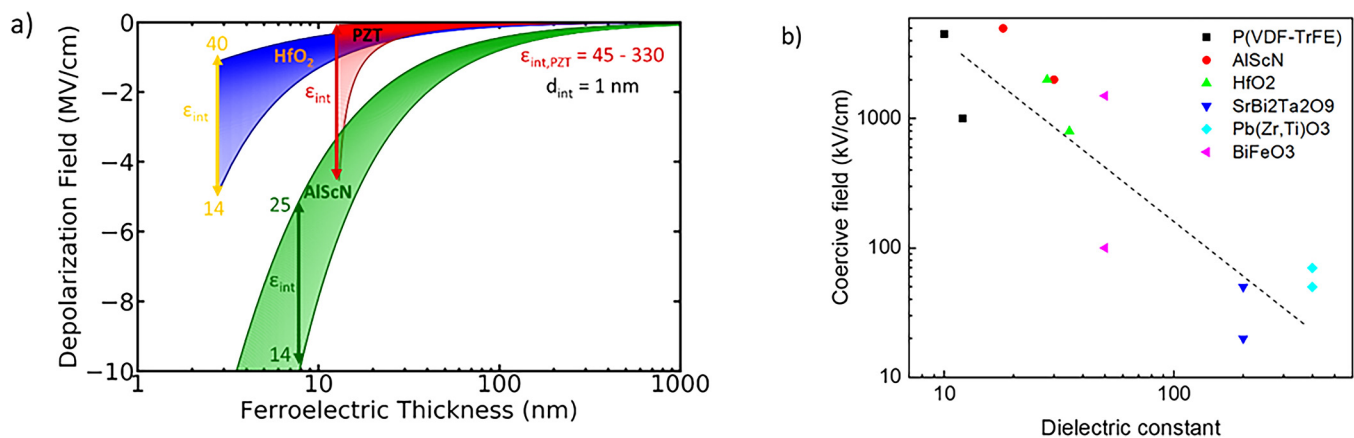


**FIG. 6.** (a) Depolarization field as a function of film thickness for PZT, doped HfO<sub>2</sub>, and Al<sub>x</sub>Sc<sub>1-x</sub>N assuming an interface layer of 1 nm to the electrodes. The dielectric constant of the ferroelectric materials was fixed to medium values of the ones given in Table I. (b) Dielectric constants of the interface are plotted for coercive field vs dielectric constant for various ferroelectric materials of Table I.

properties resulting from oxygen vacancy redistribution and/or local phase transitions;<sup>70</sup> and (4) charge injection into interfacial layers between electrode and dielectric due to the high  $E_c$ .<sup>47,70</sup> Accordingly, the high  $E_c$  is a double-sided sword of fluorite-structure ferroelectrics. On one hand, it enables achieving sufficient FeFET memory window even for sub-10-nm thickness or good retention statistics, but on the other hand, the high required field causes field-induced charge injection and limits cycling endurance by generation, redistribution, and accumulation of defects. When fluorite-structure ferroelectrics are adopted in FeFETs, the charge trapping and interfacial trap generation is even more severely limiting endurance.<sup>108,109</sup> The difference in relative dielectric constant ( $\epsilon_r$ ) of the ferroelectric and the interfacial layer (most frequently SiO<sub>2</sub> having a relative dielectric constant of  $\sim 3.9$ ) is deceived here.<sup>110</sup> While the much lower dielectric constant of hafnium oxide compared to perovskite is already a big advantage here, further decreasing the  $\epsilon_r$  of the ferroelectric layer or increasing the  $\epsilon_r$  of the interfacial layer as well as improving interfacial quality can be possible solutions. In addition, TiN is often used as an electrode material and anneals during device fabrication can reduce the ferroelectric layer at the interface and, therefore, locally degrade the material.<sup>111</sup>

Here, AlScN can have a clear advantage. Since the material is a nitride, a good stability to nitride-based electrodes is expected, which would result in thinner interface layers and reduced depolarization fields. Compared to HfO<sub>2</sub>-based dielectrics, the material typically consists of a single phase, which has the advantage that films with high ferroelectric phase fractions can be grown more easily.<sup>8</sup> AlScN is lead-free and CMOS back-end of line compatible. Due to similarities in lattice structure and unit cell size, a simple growth on GaN based substrates is expected. So far, the thinnest reported film thickness values are in the range of about 30 nm, but even thinner films are expected in the near future. First attempts in thinning down of the AlScN layer led to performance degradation,<sup>100</sup> and future work is necessary to improve the properties.

First, promising field cycling performance up to  $10^5$  cycles was demonstrated,<sup>8</sup> but also due to the early development stage, still significant improvements are expected.

## IV. FERROELECTRIC APPLICATIONS

### A. Semiconductor memories

Conventional semiconductor memory technologies such as static random access memory (SRAM), DRAM, and FLASH face scaling challenges below 22 nm nodes. Several strategies aiming to overcome them have been adopted. For example, 3D-integration ensures continuous cost per bit scaling of NAND FLASH. New high-k dielectric and electrode materials and manufacturing processes guaranteeing a thickness uniformity of a few Angstroms push DRAM scaling. SRAM scales continuously with CMOS. Besides that, the non-charge storage-based memories such as phase change memory (PCM), magnetoresistive random access memory (MRAM), resistive random access memory (ReRAM), and perovskite-based FeRAM, although in small volume commercial production, suffer from high costs. Ferroelectricity in doped hafnia opens the opportunity to overcome these integration and scaling issues due to CMOS compatibility and relative low permittivity. Three flavors of ferroelectric (FE) devices are under consideration for memory application—the 1T1C FeRAM, 1T FeFET, and the FTJ concept that are illustrated in Fig. 7.

All three device concepts store the data in a polarization state in the ferroelectric (FE) layer. Write operation is performed by applying a suitable electrical field. That makes the write operation an inherently power efficient process. The nucleation limited switching process of the ferroelectric<sup>112</sup> gives rise to a time-voltage trade-off for polarization reversal. However, the switching of ferroelectric hafnium oxide (HfO<sub>2</sub>) films in the ns-regime has already been demonstrated.<sup>108</sup> In the 1T1C concept [Fig. 7(a)], the capacitor typically consists of a metal-ferroelectric-metal (MFM) stack. For the typical coercive field of 1–2 MV/cm and ferroelectric layer thicknesses of 5–10 nm, a switching voltage in the range of 1–2 V

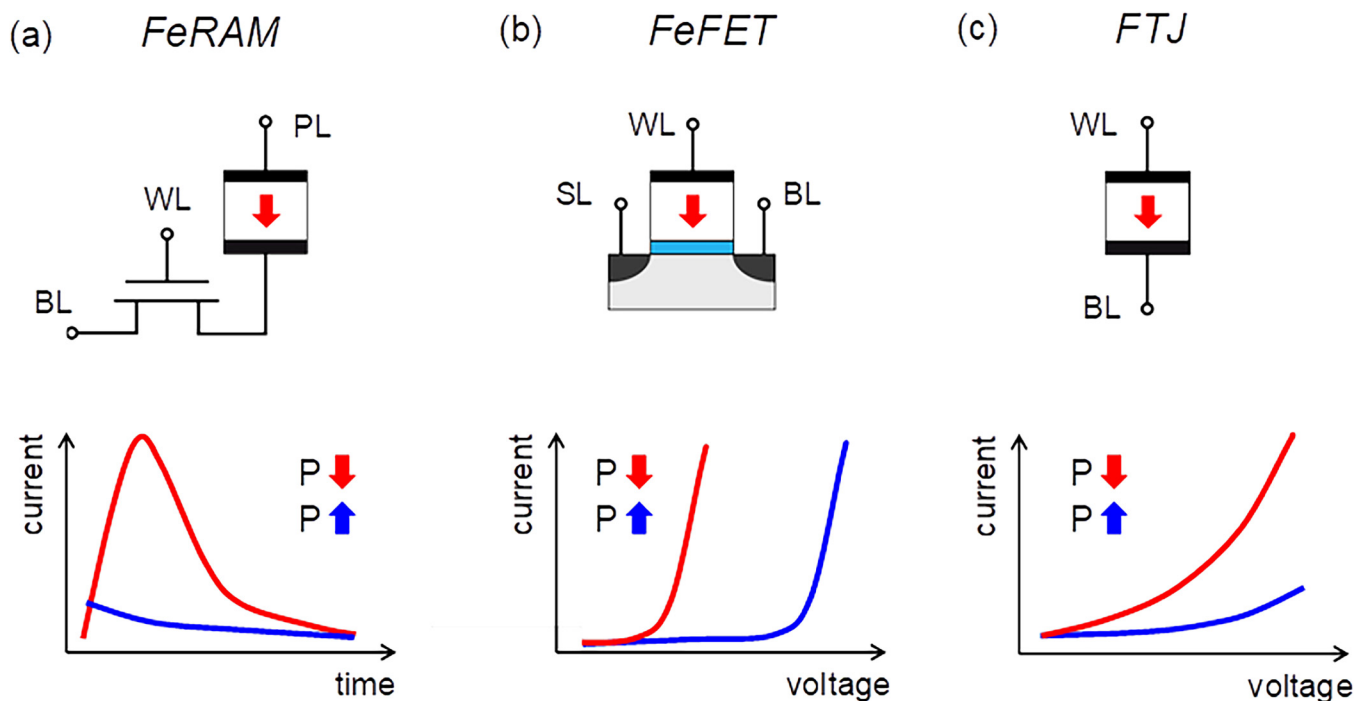


**FIG. 7.** Three ferroelectric memory concepts and their respective current-response as a function of time or voltage for both polarization directions: (a) FeRAM, (b) FeFET, and (c) FTJ.

is mandatory. In contrast, FTJ and FeFET devices typically feature additional internal dielectric layers [metal/ferroelectric/insulator/metal (MFIM) or metal/ferroelectric/insulator/semiconductor (MFIS) stack] causing an additional voltage drop and increased write voltages of 2–4 V. Nevertheless, that is about four times less compared to typical programming voltages for floating gate or charge trapping FLASH devices. While programming is very similar for the three ferroelectric device concepts, the main differentiator for memory application is the read operation.

In the 1T1C FeRAM during a destructive readout, the switched polarization charge is transferred via a select transistor to the bit line (BL) [Fig. 7(a)]. Similar as in DRAM, a sense amplifier determines the stored logic state. The readout cycle needs to be completed by restoring the information. Thus, every read cycle adds to the write endurance as well. Using PZT as the ferroelectric, an unlimited cycling endurance can be achieved.<sup>106</sup> For the better scalable hafnium oxide-based films, a cycling endurance of above  $10^{11}$  switching cycles has been demonstrated.<sup>39,113</sup> Compared to high-density standalone DRAM, due to the higher polarization charge density, a reduction of the capacitor area by a factor of 8 can be attained,<sup>114</sup> thus leading to a reduction in manufacturing complexity and consequently in the cost per bit. Successful implementations of 1T1C memory arrays have been recently demonstrated.<sup>39,115</sup> Moreover, in Ref. 116, it was proposed that the small charge signal can be amplified sufficiently by a second transistor that is added to the memory cell, thus forming a 2T1C cell, offering a reduction of the manufacturing complexity for a planar capacitor

to a minimum, however, at the cost of an increased memory cell size. Further development will focus on the scaling and 3D integration<sup>38</sup> together with the optimization of capacitor reliability that is mandatory for manufacturing of memory arrays with several Gbits in density.

In the 1T FeFET memory concept, the polarization charge of the ferroelectric gate oxide material controls the threshold voltage of the transistor and thus its channel conductivity. Hence, making use of the transistors internal gain, a non-destructive readout operation can be achieved by sensing the drain-source-current, while still the stored data can be maintained in a nonvolatile manner.<sup>7</sup> Successful integration of the hafnium oxide-based FeFETs into commercial planar 28 nm and 22 nm state-of-the-art high-k metal gate technologies was demonstrated.<sup>108,117,118</sup> Today, the cycling endurance is still at the edge of what is required for a nonvolatile memory<sup>110</sup> mainly caused by the degradation of the interfacial layer that forms between the Si channel and the ferroelectric layer.<sup>119</sup> However, the reported endurance of  $10^4$  for gate first process<sup>119</sup> and up to  $10^7$  write cycles for gate last process<sup>120</sup> can compete with conventional floating gate and charge trapping devices and makes the FeFET device very suitable as an embedded nonvolatile memory (eNVM) solution. The further improvement of the cycling endurance might be attained by eliminating the interfacial oxide layer using different channel materials such as Ge<sup>121</sup> or conductive metal oxides<sup>122</sup> or by device structure engineering that changes the capacitive voltage divider between the ferroelectric and dielectric layers.<sup>110</sup> In terms of cost per bit, mainly three aspects are decisive. First, from array disturb analysis, AND or

NOR type array architectures are preferred,<sup>123,124</sup> implying a larger cell size compared to NAND. Second, the poly-crystallinity of the ferroelectric material causes a certain variability in the switching characteristic that typically is counteracted by increasing transistor size beyond  $0.01 \mu\text{m}^2$ ,<sup>108,118</sup> so far hindering the scalability of the concept to feature sizes that can compete with standalone memories. Improvement could be attained by the application of textured or epitaxial grown ferroelectric films.<sup>56</sup> Third, storing multiple bits in one FeFET was successfully demonstrated.<sup>125</sup> However, in the FeFET case, the multi-level storage is limited by the maximum achievable threshold voltage memory window (MW) as calculated from a first-order estimation by  $\text{MW} = 2 * E_c * t_{\text{ox}} \sim 2 \text{ V}$  and the realization of more than 2 bits per cell seems not realistic. A way to enlarge the MW is to increase the thickness of the FE layer as demonstrated in Ref. 126.

The scalability limitations could be overcome by the realization of high-density 3D-NAND FeFET memories.<sup>127</sup> Besides a larger effective gate area of the FeFET gate that would improve multi-level storage compared to the planar FeFET, an increased array efficiency could be attained due to lower on-chip generated programming voltages for the FeFET when compared to FLASH devices. However, cycling endurance might be the critical factor here as well.

In the third device concept, the ferroelectric tunnel junction (FTJ), that was first proposed by Esaki *et al.* in 1970s as a “polar switch,”<sup>31</sup> the polarization state of the device is detected by measuring the current flow upon application of an electrical field that is smaller than the coercive field of the ferroelectric. The change in the tunneling current is called the tunneling electroresistance (TER) and is measured as the ratio between the resistance of the device in the low resistance state (LRS) and the high resistance state (HRS). Typical values range from 2 to 100. Similar to FeFET, the FTJ allows a non-destructive read operation. Different mechanisms that might contribute to the resistance change effect in the FTJ have been studied.<sup>128,129</sup> Typically, a higher tunneling electroresistance (TER) ratio can be attained for a thicker ferroelectric layer, thus causing a trade-off with the attainable current density that decreases with increasing the ferroelectric layer thickness. Hence, the main obstacle to overcome in fabricating FTJ devices is the formation of an ultra-thin ferroelectric layer. The idea of the composite barrier or double layer FTJ is to separate the tunneling effect and the ferroelectric switching effect from each other,<sup>41,130–132</sup> thus yielding larger TER ratio while not degrading the current density. Typical values are in the range of  $1 \mu\text{A}/\text{cm}^2$ .<sup>131</sup> A precise control of both thickness of the ferroelectric and dielectric layer is of utmost importance for proper FTJ functionality.<sup>131,133</sup>

Scaling the FTJ to the nm-regime results in very small read currents below 1 pA. That is, comparatively long read times are mandatory that conflict with typical memory requirements. Hence, the main application of FTJs is seen in neuromorphic applications where a massive parallel operation of multiple devices is required.<sup>134,135</sup>

In summary, from the current perspective, two realizations of hafnium oxide-based ferroelectric memories are likely to enter the market in the foreseeable future. For standalone devices, a memory type storage class device based on the 1T1C concept, featuring close to DRAM-like performance in terms of speed and density but at reduced endurance, is the most likely case. Due to low cost implementation, the 1T FeFET concept integrated into

high-k metal gate technology is a very attractive candidate in terms of low power and cost per bit. Additionally, reasonable cycling endurance and fast access times makes the concept very likely to find first niche applications that pave the way into the eNVM market. The very low current density of the FTJ devices limits the speed of the read operation but enables massive parallel processing. Recently, there also have been considerable efforts to utilize FeFETs and FTJ in in-memory computing as well as realizing artificial neurons and synapses for neuromorphic computing systems. In-memory computing using FeFETs was investigated in Refs. 136, 138, 214, 215 and for FTJs in Ref. 139. Synapses for neuromorphic computing using FeFETs are described in Refs. 140–142 and using FTJs in Refs. 143 and 144. Finally, in Ref. 145, it was shown that the accumulative switching observed in scaled down FeFETs can be used to mimic biological neurons. Finally, the functionality of the FeFET can also be used for non-memory tasks like frequency multiplication as described in Ref. 210.

## B. Negative capacitance

One of the most prominent problems in nanoelectronics is the inability to reduce the supply voltage when further scaling device dimensions, which leads to increased power dissipation.<sup>146</sup> This is caused by the thermal broadening of the Fermi–Dirac distribution of electrons.<sup>147</sup> One could overcome this limit by using a negative capacitance (NC) material, which would internally amplify the voltage applied to a transistor.<sup>42</sup> Theoretically, this could be achieved by using a ferroelectric gate insulator, which needs to be thin enough to be stabilized in a state of NC. While the structure of such an NC field-effect transistor (NCFET) is similar to a memory FeFET, both are conceptually different. While a FeFET operates by switching the ferroelectric between two stable polarization states, the NCFET only has one stable state for each applied voltage and thus should exhibit no hysteresis. This idea of stabilized NC must be distinguished from transient NC phenomena, which occur during ferroelectric polarization switching and involve hysteresis.<sup>148–150</sup>

Stabilized NC has been mainly reported in epitaxial ferroelectric/dielectric perovskite heterostructures and superlattices and seems to emerge from complex domain topologies.<sup>7–12</sup> Therefore, single-domain models are often insufficient to describe such effects.<sup>151</sup> Transient NC has been demonstrated in metal–ferroelectric–metal (MFM) capacitors utilizing perovskites as well as  $\text{HfO}_2$  and polymer based ferroelectrics.<sup>152–154</sup> It has been established that transient NC effects occur when the spontaneous polarization changes faster than the free screening charge, independent of the specific switching mechanism.<sup>155,156</sup> However, the inherent instability of the NC state in MFM capacitors is unfavorable for NCFET applications.<sup>157,158</sup> Therefore, to stabilize NC, it seems necessary to bring the ferroelectric into direct contact with a dielectric layer.

Recent experiments on ferroelectric/dielectric capacitors suggest that hysteresis-free NC in  $\text{HfO}_2$ -based materials is achievable.<sup>159–161</sup> However, large layer thicknesses and interface charges necessitate high applied voltages.<sup>162</sup> Therefore, using ultra-thin ( $<2 \text{ nm}$ )  $\text{HfO}_2$ -based ferroelectrics might be necessary going forward.<sup>163</sup> Experimental reports indicate that such NCFETs can show improved ON/OFF ratio or lower supply voltage as well as mitigate short-channel effects in scaled devices.<sup>164–166</sup> Nevertheless, reducing the

supply voltage below the thermal limit without hysteresis seems to be challenging.<sup>167</sup> One reason for this is that NC in HfO<sub>2</sub>-based ferroelectrics is not well understood so far and more elaborate models based on microscopic insights are needed for NCFET design.<sup>44</sup> Finally, the growth of more homogeneous and phase pure ultra-thin ferroelectric HfO<sub>2</sub> films is still an issue, which needs to be a focus of future research.

### C. Energy-related applications

In ferroelectric materials, the characteristic spontaneous polarization originates from the changes in relative positions of cations and anions, so their polarization is strongly affected by mechanical stress and temperature.<sup>168–172</sup> The piezoelectricity and pyroelectricity of ferroelectric materials originate from electro-mechanical and electrothermal coupling, respectively, which can be utilized for the conversion between electrical energy and mechanical or thermal energy. Therefore, the piezoelectricity and pyroelectricity can be utilized for various applications such as energy harvesters, sensors, solid-state-coolers, actuators, and electrostatic supercapacitors, and conventional ferroelectric materials have been intensively studied for these applications. Although size-dependences in piezoelectricity and pyroelectricity as well as electrical bandgap higher than 5 eV of fluorite-structure ferroelectrics are not most suitable for the large-scale energy conversion and photovoltaic applications, their nanoscale energy conversion based on emerging piezoelectricity and pyroelectricity is paving a way for new applications. In this section, various energy-related applications of emerging fluorite-structure ferroelectrics are reviewed, and perspectives on the applications are provided.

In 2014, Park *et al.*<sup>173</sup> suggested that the field-induced phase transition in Zr-rich Hf<sub>1-x</sub>Zr<sub>x</sub>O<sub>2</sub> thin film could be utilized as electrostatic supercapacitors, which can support the energy storage systems. The field-induced phase transition could significantly increase the energy storage density (ESD) compared to linear dielectric thin films due to large difference in polarization of non-polar and polar phase. As shown in Fig. 8(a), the ESD up to 46 J/cm<sup>3</sup> could be achieved in Hf<sub>0.3</sub>Zr<sub>0.7</sub>O<sub>2</sub> thin films. The ESD value of 30 J/cm<sup>3</sup> could be reliably achieved up to 175 °C, which was the limitation of experimental setup as shown in Fig. 8(b), and the endurance up to 10<sup>9</sup> charging/discharging cycles could be also confirmed as shown in Fig. 8(c). Hoffmann *et al.*<sup>172</sup> also showed that 5.6 mol. % Si-doped HfO<sub>2</sub> could show high ESD up to 40 J/cm<sup>3</sup> with an efficiency of 80%. Kim *et al.*<sup>174</sup> reported ESD up to 47 J/cm<sup>3</sup>, and such high value could be attributed to the stress induced by the top TiN electrode. Pesic *et al.*<sup>175</sup> reported that three-dimensional electrostatic supercapacitors with antiferroelectric ZrO<sub>2</sub> and ESD of 930 J/cm<sup>3</sup> per projected 2D capacitor area could be achieved. Hoffmann *et al.*<sup>162</sup> suggested that the negative capacitance of ferroelectric doped HfO<sub>2</sub> can be utilized for electrostatic supercapacitor with high ESD even up to 120 J/cm<sup>3</sup>. The ESD values of electrostatic supercapacitors based on fluorite-structure antiferroelectrics and several other pyroelectric materials are summarized in Fig. 8(d).<sup>176–180</sup> Despite the rather short research history of 6 years, the ESD value of fluorite-structure antiferroelectrics are comparable or even better than those achieved by conventional materials.

The pyroelectricity in fluorite-structure antiferroelectrics is another interesting aspect for various applications. Fluorite-structure ferroelectrics are currently known as the first-order-phase-transition materials, so the field-induced phase transition can be observed during the phase transition above T<sub>c</sub>, which can be controlled by doping concentration.<sup>171,172</sup> Figures 8(e) and 8(f) show the x-ray diffraction patterns and P-E curves of Si-doped HfO<sub>2</sub> thin films measured at various temperatures, demonstrating first-order phase transition between *Pca*2<sub>1</sub> orthorhombic and *P4*<sub>2</sub>/*nmc* tetragonal phases.<sup>62</sup> Pandya *et al.*<sup>169</sup> first demonstrated that the large entropy difference between the tetragonal and orthorhombic phase [see P-E curves in Fig. 8(g)] enables the giant pyroelectric energy harvesting (harvestable energy density HED up to 11.5 J/cm<sup>3</sup> cycle) and electrocaloric effect [adiabatic temperature change  $\Delta T$  up to 13.4 K, Fig. 8(g)]. Hoffmann *et al.*<sup>172</sup> also reported that the phase transition in Si-doped HfO<sub>2</sub> can be controlled by engineering Si concentration as shown in Fig. 8(i), and the  $\Delta T$  and HED values up to 9.5 K and 20 J/cm<sup>3</sup> cycle could be achieved. Park *et al.* examined the effect of dopant species on the phase transition and resulting electrocaloric effect in HfO<sub>2</sub> and suggested that the four valent dopants could show higher  $dP_r/dT$  values and resulting higher  $\Delta T$  values. The reports on electrocaloric effect and pyroelectric energy harvesting are summarized in Figs. 8(k) and 8(l), respectively. The pyroelectricity of fluorite-structure ferroelectrics have been suggested to be utilized for IR sensors based on pyroelectricity. Mart *et al.*<sup>181</sup> examined the pyroelectric coefficient of Si-doped HfO<sub>2</sub> with various film thicknesses and the maximum pyroelectric coefficient  $p$  of  $-84 \mu\text{C}/\text{m}^2 \text{K}$  could be achieved; this value was comparable to that of LiNbO<sub>3</sub>. Moreover,  $p$  of  $-80 \mu\text{C}/\text{m}^2 \text{K}$  and  $-58 \mu\text{C}/\text{m}^2 \text{K}$  were reported for La-doped HfO<sub>2</sub><sup>182</sup> and Hf<sub>1-x</sub>Zr<sub>x</sub>O<sub>2</sub><sup>183,184</sup> thin films. Although  $p$  of fluorite-structure ferroelectrics is lower than those of lead-containing ferroelectrics such as Pb(Zr,Ti)O<sub>3</sub> or PMN-PT, they can be considered promising candidates among environmental-friendly lead-free pyroelectrics.

### D. Sensor and actuator related application

A variety of sensor and actuator applications utilize the direct and converse piezoelectric effect as well as the pyroelectric effect produced from ferroelectric materials. The CMOS compatible chemistries of HfO<sub>2</sub>-based and Al<sub>x</sub>Sc<sub>1-x</sub>N ferroelectrics offer feasible routes to integrate piezoelectric-based micro-electro-mechanical systems (MEMS) and circuits into monolithic designs. Advances in inkjet printing, radio frequency (RF) filters and resonators, miniaturized robotics, and adaptive optics will benefit from progress made in next generation piezoelectric materials.<sup>186,187</sup> Cost effective microgyrosensors employing piezoelectrics for inertial and motion sensing have already seen success in commercial and industry applications, but further material development can make them more competitive for higher precision grades. The pyroelectric effect generated from ferroelectrics serves as the basis in infrared sensors and arrays for motion sensing and thermal imaging applications.

Ferroelectricity in HfO<sub>2</sub>-based thin films was first reported in 2011<sup>6</sup> and intense interest in incorporating FE HfO<sub>2</sub> for a variety of ferroelectric nonvolatile memory applications at first overshadowed studies looking at the pyroelectric and piezoelectric effect in the



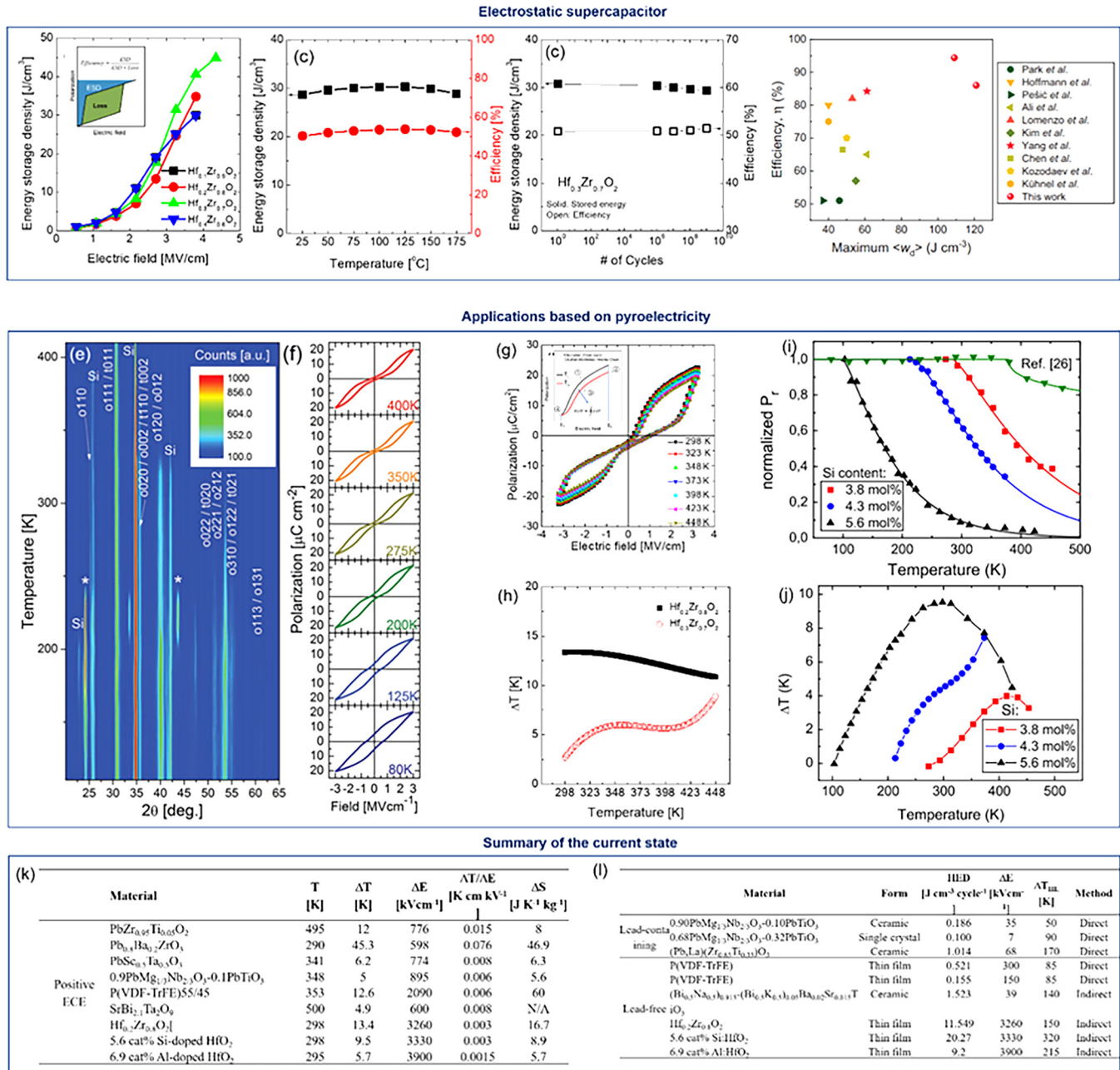


**FIG. 8.** Electrostatic supercapacitors based on fluorite-structure ferroelectrics. (a) The polarization electric field curve of  $\text{Hf}_{1-x}\text{Zr}_x\text{O}_2$  films with various compositions with schematic mechanism for energy storage using antiferroelectricity (inset). (b) Energy storage density of  $\text{Hf}_{1-x}\text{Zr}_x\text{O}_2$  films. (c) Thermal stability and (d) endurance of electrostatic supercapacitor with  $\text{Hf}_{0.3}\text{Zr}_{0.7}\text{O}_2$  thin film. (e)–(j) Applications based on pyroelectricity of fluorite-structure ferroelectrics. (e) A color contour map constructed based on x-ray diffraction patterns and (f) polarization–electric field (P–E) curves of Si-doped  $\text{HfO}_2$  thin film measured at various temperatures. (g) P–E curves and (h) adiabatic temperature change of  $\text{Hf}_{0.2}\text{Zr}_{0.8}\text{O}_2$  thin films. (i) Temperature-dependent normalized remanent polarization ( $P_r$ ) and  $\Delta T$  of Si-doped  $\text{HfO}_2$  thin films with various doping concentrations. Summary of (k) electrocaloric effect and (l) pyroelectric energy harvesting reported in the literature. (a)–(c) Reproduced with permission from Park *et al.*, *Adv. Energy Mater.* **4**(16), 1400610 (2014). Copyright 2014 John Wiley and Sons. (d) Reproduced with permission from Hoffmann *et al.*, *Adv. Energy Mater.* **9**, 1901154 (2019). Copyright 2019 Elsevier. (e) and (f) Reproduced with permission from Park *et al.*, *Adv. Electron. Mater.* **4**, 1700489 (2018). Copyright 2018 John Wiley and Sons. (g) and (h) Reproduced with permission from Park *et al.*, *Nano Energy* **12**, 131–140 (2015). Copyright 2015 Elsevier. (i) and (j) Reproduced with permission from Hoffmann *et al.*, *Nano Energy* **18**, 154–164 (2015). Copyright 2015 Elsevier. (k) and (l) From Park *et al.*, “Pyroelectric and electrocaloric effects and their applications,” in *Ferroelectricity in Doped Hafnium Oxide: Materials, Properties and Devices*. Copyright 2019 Elsevier. Reprinted with permission from Elsevier.

early years after its discovery. Since then, progress has been made evaluating the pyroelectric coefficient in ferroelectric  $\text{HfO}_2$  with a variety of dopants,<sup>182,184,188</sup> film thicknesses,<sup>181,183</sup> temperature and frequency ranges.<sup>184,188,189</sup> The influence of Si-doping concentration and different dopants on the pyroelectric coefficient is shown in Figs. 9(d) and 9(e). Pyroelectric coefficients in the range of  $40\text{--}84\text{ }\mu\text{C m}^{-2}\text{ K}^{-1}$  have been observed in  $\text{HfO}_2$ -based films, which is comparable to the high-performance pyroelectric lithium niobate. Wake-up and secondary effects appear to have an influence on the pyroelectric performance of ferroelectric  $\text{HfO}_2$  and further investigations are warranted to better understand such effects fundamentally as well as the implications for IR sensor development.<sup>181,183,189</sup> The demonstration of 3D integrated  $\text{HfO}_2$  pyroelectric deep trench capacitors is promising for high performance integrated IR arrays.<sup>190</sup> Early reports of the pyroelectric coefficient in  $\text{Al}_x\text{Sc}_{1-x}\text{N}$  have observed a pyroelectric coefficient in the range of  $5\text{--}10\text{ }\mu\text{C m}^{-2}\text{ K}^{-1}$ , which is similar to the relatively low pyroelectric coefficient measured in pure AlN.<sup>191,192</sup>

Piezoelectric AlN bulk acoustic wave (BAW) resonators and RF filters have become essential components for front end RF wireless communication devices over the last decade.<sup>193</sup> Due to the high Q factors of AlN film bulk acoustic resonators (FBARs), further progress in improving the properties of AlN-based films will be important for incorporating these devices into next generation wireless communication modules. Doping AlN with Sc can enhance its piezoelectric properties and electro-mechanical coupling, but because Sc doping causes a consequent decrease in the sound velocity and resonator quality, an improved bandwidth comes at the cost of a less steep filter skirt.<sup>194</sup> Acoustically coupled  $\text{Al}_{0.7}\text{Sc}_{0.3}\text{N}$  RF filters operated at 2.3 GHz have been demonstrated with a  $-3\text{ dB}$  bandwidth of  $70\text{--}115\text{ MHz}$ , which is three times larger than state-of-the-art AlN acoustically coupled RF filters.<sup>195</sup> Sc doping of AlN leads to dramatic increases in the  $d_{33}$  piezoelectric coefficient from approximately  $5\text{--}30\text{ pm/V}$  with increasing Sc doping.<sup>196</sup>

The piezoelectric properties of  $\text{HfO}_2$  have only received attention since the discovery of ferroelectricity in 2011 with piezoelectric

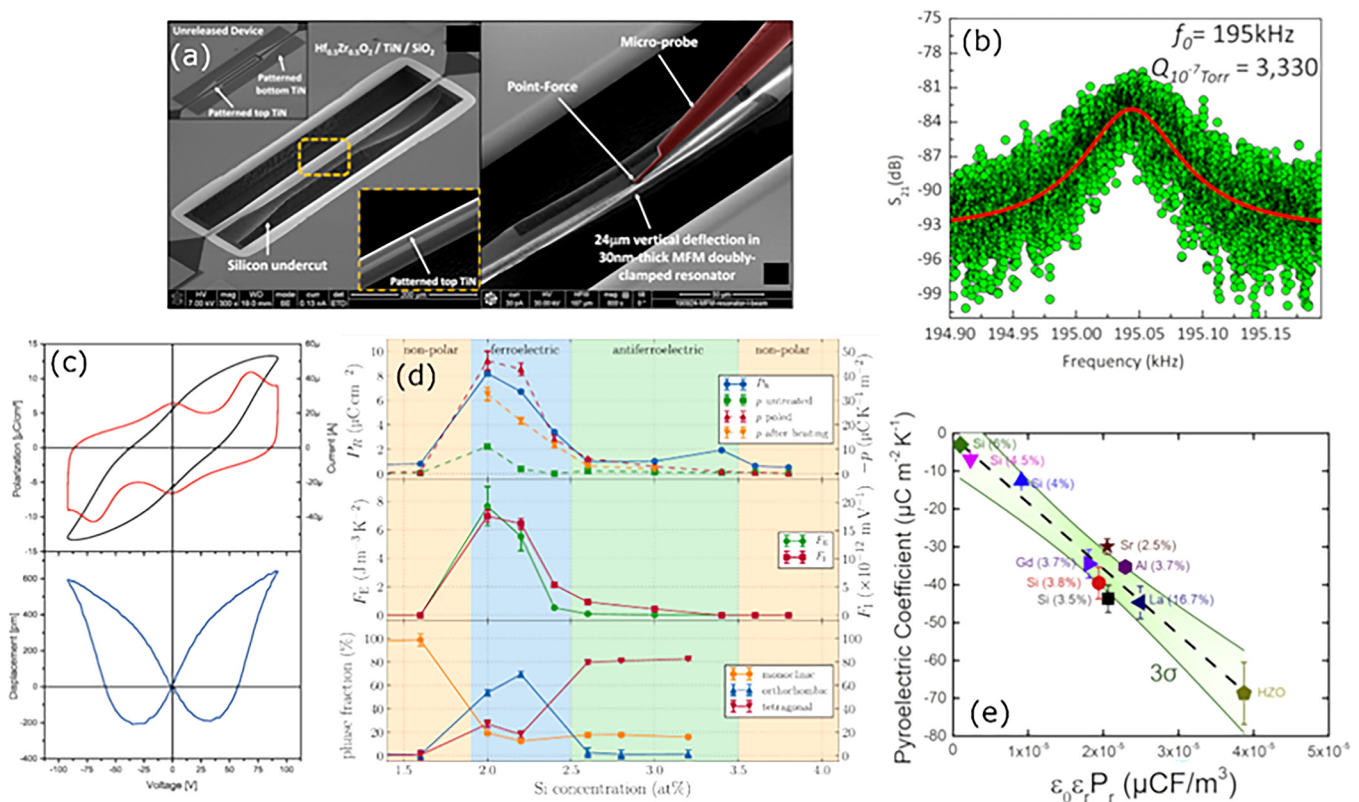


**FIG. 9.** (a) and (b) Resonator with 10 nm thick  $\text{Hf}_{0.5}\text{Zr}_{0.5}\text{O}_2$  and microprobe showing mechanical robustness with a high Q factor of 3300 at  $10^{-7}$  Torr. (c) Displacement vs electric field laser interferometry measurements of Si-doped  $\text{HfO}_2$  with thicknesses in the 10 nm–50 nm range and displacement curves measured from a 390 nm thick  $\text{ZrO}_2$  film. (d) Remanent polarization, pyroelectric coefficient,  $F_E$  and  $F_I$  figures of merit for energy harvesting and IR applications, and phase fraction with Si-doped in Si- $\text{HfO}_2$  thin films. (e) SEM image of deep trench pyroelectric capacitors using Si-doped  $\text{HfO}_2$  thin films. (f) Pyroelectric coefficient vs  $\epsilon_0\epsilon_r P_r$  for La, Si, Gd, Sr, Al, and Zr doped  $\text{HfO}_2$  thin films. (a) and (b) Reproduced with permission from Ghatge *et al.*, Nat. Electron. **2**(11), 506–512 (2019). Copyright 2019 Springer Nature. (c) Reproduced with permission from Starschich *et al.*, Appl. Phys. Lett. **110**, 182905 (2017). Copyright 2017 AIP Publishing LLC. (d) Reproduced with permission from Jachalke *et al.*, Appl. Phys. Lett. **112**, 142901 (2018). Copyright 2018 AIP Publishing LLC. (e) Reproduced with permission from Lomenzo *et al.*, Nano Energy **74**, 104733 (2020). Copyright 2020 Elsevier.

coefficients ( $d_{33}$ ) being reported in the range of 10–20 pm/V.<sup>197–199</sup> Thick HZO films deposited by chemical solution deposition (CSD) appear to be promising for larger total displacements [Fig. 9(c)]. Nano-electro-mechanical systems (NEMS) devices appear to be particularly promising for extremely high precision actuators and transducers. Large vibrational amplitudes of 100 nm have been achieved with 10 nm thick  $\text{Hf}_{0.5}\text{Zr}_{0.5}\text{O}_2$  incorporated into a NEMS resonator with a Q factor of 3300<sup>200</sup> at  $10^{-7}$  Torr as shown in Figs. 9(a) and 9(b). Resonators with frequencies up to 13 GHz were achieved using 10 nm ferroelectric  $\text{Hf}_{0.5}\text{Zr}_{0.5}\text{O}_2$ .<sup>201,202</sup> While the monoclinic phase generally degrades the ferroelectric and piezoelectric properties of ALD grown  $\text{HfO}_2$  films at thicknesses greater than 15 nm, chemical solution deposition (CSD) and epitaxial film growth has demonstrated films in the thickness range of 100 nm– $\mu\text{m}$ .<sup>53,203,204</sup> Such thicker piezoelectric films can be beneficial for some applications since the total mechanical displacement increases as the film thickness grows.

Overall,  $\text{HfO}_2$ -based and AlScN piezoelectric and pyroelectric materials offer new opportunities to further extend MEMS, NEMS, and sensor device functionalities. The ability to integrate both materials into a CMOS process with already established conformal deposition techniques circumvents many of the difficulties and hurdles that prevent the integration of perovskite ferroelectrics. Further optimization of the piezoelectric and pyroelectric properties in both materials through process innovations, chemical doping, and device engineering will be an important area of research over the next decade for commercial and industrial implementation of these materials.

## E. Device perspectives

For the discussion on ferroelectric devices, we will discriminate between the devices that make explicit use of the ferroelectricity, i.e., the property of the crystal to allow reversible switching between two stable polarization states and the devices that use a property that is connected with ferroelectricity like pyroelectricity, piezoelectricity, or a high permittivity since both groups have different starting points. The dominating application for the former group is semiconductor memories. This requires integration with CMOS support circuitry. In contrast, many devices that rely on high permittivity, pyroelectricity, or piezoelectricity are established on the market but are generally using either bulk crystals or specialized thin film technologies that are not totally compatible with CMOS. When it comes to memories, it has been mentioned a few times that FeRAM using PZT or SBT is established in niche markets.<sup>5,28,205</sup> Although promising demonstrations of hafnium oxide-based FeRAMs have been made,<sup>39,115</sup> the high coercive field and the associated difficulty in achieving a stable cycling as well as a stable retention and imprint behavior are still significant challenges for integrating this material into an FeRAM that fulfills all requirements for a RAM type memory. Specialized products that possibly compromise some of the full specifications like endurance or minimum cell size could be a door opener here. For embedded memory applications, the 2T/1C gain cell proposed in Ref. 116 could be a way to save process complexity at the cost of cell size. Moreover, using the antiferroelectric hysteresis that can be achieved in hafnium oxide and zirconium oxide, the limitations may also be

overcome.<sup>175,206–208</sup> Whether AlScN can break into this domain needs to be seen, when more data and better understanding of the optimization for that material is available. The FeFET seems to be a natural fit for hafnium oxide-based ferroelectrics, since state-of-the-art MOSFETs already use  $\text{HfO}_2$  as the gate dielectric and, therefore, the device can be integrated with little additional effort.<sup>118</sup> The current status makes it possible to see a product with NOR Flash specification for the embedded NVM market in the foreseeable future. To achieve this goal, variability and reliability need to be mastered. To the later end, the high coercive fields are an issue here. They not only lead to the already mentioned endurance cycling limitations and rather high switching voltages for FeRAM but are also a concern with respect to charge injection both during switching and storage. On top of the limited endurance, imprint is a topic that needs to be mastered here.<sup>209</sup> From there on, further widening of the specification can lead to memories that will significantly outperform NOR Flash. Again, the 2T/1C approach could be a viable complement having larger cell size together with higher endurance. Finally, FTJ is still in its infancy. Note that ferroelectric memory devices cannot only be used for the prime memory function as described above but are also ideally suited for overcoming the so-called von-Neuman bottleneck<sup>133</sup> in concepts like in-memory computing<sup>136,137</sup> or as synapses<sup>142</sup> or neurons<sup>145</sup> in neuromorphic systems. Moreover, the nonvolatile memory function can also be used to tailor device properties on demand as has been recently demonstrated in a reconfigurable frequency multiplier.<sup>210</sup>

The other applications making direct use of the ferroelectric properties are negative capacitance and supercapacitors. While it is still doubtful, if a device showing the theoretical improvements expected from the negative capacitance can actually be achieved, given the large amount of research that was put into this topic in the last 5 years, the research could still lead to some improvements in other fields and possibly help improve the performance of supercapacitors.<sup>162</sup> Moreover, antiferroelectric hysteresis could be utilized for integrated supercapacitor as well.<sup>175</sup>

The starting point and perspectives for sensor, actuator, and energy harvesting devices based on the properties of piezoelectricity and pyroelectricity are fundamentally different because of two aspects. First, there is a wealth of applications already on the market using these effects in traditional ferroelectric or piezoelectric materials either in the form of bulk crystals or in the form of thin film technology that is not integrated together with state-of-the-art electronics. As a result, the market for such products is well defined and displacing a successful material will only happen if there is a large performance or cost advantage. The new quality that comes with ferroelectrics that are fully compatible with electronics device fabrication is the possibility to integrate the sensor, actuator, or energy harvesting devices directly into a monolithic integrated system. While it seems that there is still a very significant competitive edge for hafnium oxide-based ferroelectrics in the field of memories and related devices, here AlScN has a very strong starting position, since AlN is already in use and the shift is not so far. In any case, widespread utilization of the new materials will take significantly longer time compared to memories and related devices, since we are talking about a very fragmented segment and the benefits need to be demonstrated device by device. Once a critical mass is achieved, this



development could lead to ferroelectric devices utilizing several physical effects being standard elements in highly integrated systems and, therefore, could initiate an avalanche of new low cost applications.

## V. SUMMARY AND OUTLOOK

In summary, the appearance of fully CMOS compatible ferroelectric materials for use in both the front end and the back end of line processes has inspired a large amount of research into using these materials in established as well as novel type devices. This development could bring ferroelectric memories out of the niche into a much more widespread application range and open new fields of using ferroelectric devices in integrated devices. After first reports about ferroelectric hafnium oxide, rapid progress has been made both in understanding the material properties and in using the material in various devices. Still some issues with regard to stability need to be solved to finally achieve breakthroughs in the application field, but these are on the horizon as research and development activities are further increasing. Very recently, with AlScN, another promising material system has been added that is ideally suited to fit into GaN based devices and is closer to a number of existing piezoelectric applications based on AlN. The prospects of these systems for memories and related devices need to be established. However, it will almost certainly find its way into sensor, actuator, and energy harvesting applications. Bringing the different streams together in future integrated circuit technologies could pave the way to a rich portfolio of ferroelectric device possibilities in future integrated circuits.

## AUTHORS' CONTRIBUTIONS

The manuscript was written through contributions of all co-authors. T.M. and S.S. have written Secs. I, II, IV A, and IV E; H.M. and S.S. have written Sec. IV A; H.M., S.S., and T.M. have written Sec. IV E; M.H.P. and U.S. have written Secs. II A, II B, and IV C; S.F. has written Sec. III C; P.D.L. has written Sec. IV D; M.H. has written Sec. IV B; and U.S. and M.H.P. have written Secs. III B and III D. All authors have given approval to the final version of the manuscript.

## ACKNOWLEDGMENTS

M.H.P. was supported by the National Research Foundation of Korea funded by the Ministry of Science and ICT (Grant Nos. 2020R1C1C1008193 and 2020M3F3A2A01081593). P.D.L. was funded by the German Ministry of Economic Affairs and Energy (BMW) Project No. 16IPCEI310. S.F. was funded by the German Federal Ministry of Education and Research (BMBF) project ForMikro-SALSA (No. 16ES1053).

## DATA AVAILABILITY

The data that support the findings of this study are available from the corresponding author upon reasonable request.

## REFERENCES

<sup>1</sup>T. Mikolajick, "Ferroelectric nonvolatile memories," *Ref. Module Mater. Sci. Mater. Eng.* (published online 2016).

- <sup>2</sup>T. Mitsui, "Ferroelectrics and antiferroelectrics," in *Springer Handbook of Condensed Matter and Materials Data*, edited by W. Martienssen and H. Warlimont (Springer, Heidelberg, 2005), pp. 903–938.
- <sup>3</sup>Y. Xu, *Ferroelectric Materials and Their Applications* (Elsevier, 1991).
- <sup>4</sup>S. Trolier-McKinstry, "Impact of ferroelectricity," *Am. Ceram. Soc. Bull.* **99**(1), 22–23 (2020), see [https://ceramics.org/wp-content/uploads/2020/01/JanFeb-2020\\_Feature.pdf](https://ceramics.org/wp-content/uploads/2020/01/JanFeb-2020_Feature.pdf).
- <sup>5</sup>T. Mikolajick, U. Schroeder, and S. Slesazek, "The past, the present, and the future of ferroelectric memories," *IEEE Trans. Electron Devices* **67**(4), 1434–1443 (2020).
- <sup>6</sup>T. S. Böске, J. Müller, D. Bräuhäus, U. Schröder, and U. Böttger, "Ferroelectricity in hafnium oxide thin films," *Appl. Phys. Lett.* **99**(10), 102903 (2011).
- <sup>7</sup>M. Bohr, R. Chau, T. Ghani, and K. Mistry, "The high-k solution: Microprocessors entering production this year are the result of the biggest transistor redesign in 40 years," *IEEE Spectr.* **44**, 29–35 (2007).
- <sup>8</sup>S. Fichtner, N. Wolff, F. Lofink, L. Kienle, and B. Wagner, "AlScN: A III-V semiconductor based ferroelectric," *J. Appl. Phys.* **125**, 114103 (2019).
- <sup>9</sup>Z. Guan, H. Hu, X. Shen, P. Xiang, N. Zhong, J. Chu, and C. Duan, "Recent progress in two-dimensional ferroelectric materials," *Adv. Electron. Mater.* **6**, 1900818 (2020).
- <sup>10</sup>M. Osada and T. Sasaki, "The rise of 2D dielectrics/ferroelectrics," *APL Mater.* **7**, 120902 (2019).
- <sup>11</sup>J. Valasek, "Piezo-electric and allied phenomena in Rochelle salt," *Phys. Rev.* **17**, 475 (1921).
- <sup>12</sup>J. Fousek, "Joseph Valasek and the discovery of ferroelectricity," in *Proceedings of IEEE International Symposium on Applications of Ferroelectrics* (IEEE, 1994), pp. 1–5.
- <sup>13</sup>G. Busch and P. Scherrer, "Eine neue seignette-elektrische substanz," *Naturwissenschaften* **23**, 737 (1935).
- <sup>14</sup>H. Thurnauer and J. Deaderick, "Insulating material," U.S. patent 2,429,588 (21 October 1947).
- <sup>15</sup>A. von Hippel, R. G. Breckenbridge, F. G. Chesley, and L. Tisza, "High dielectric constant ceramics," *Ind. Eng. Chem.* **38**(11), 1097–1109 (1946).
- <sup>16</sup>B. Wul and J. M. Goldman, "Ferroelectric switching in BaTiO<sub>3</sub> ceramics," *C.R. Acad. Sci. URSS* **51**, 21 (1946).
- <sup>17</sup>D. A. Buck, "Ferroelectrics for digital information storage and switching," MIT Digital Comput. Laboratory Report, 05 June 1952, see <https://dome.mit.edu/handle/1721.3/40244>.
- <sup>18</sup>J. R. Anderson, "Ferroelectric materials as storage elements for digital computers and switching systems," *Trans. Am. Inst. Electr. Eng. Part 1* **71**, 395–401 (1953).
- <sup>19</sup>J. Merz and J. Anderson, "Ferroelectric storage devices," *Bell Lab Records* **33**, 335–342 (1955).
- <sup>20</sup>G. Shirane and A. Takeda, "Phase transitions in solid solutions of PbZrO<sub>3</sub> and PbTiO<sub>3</sub> (I) small concentrations of PbTiO<sub>3</sub>," *J. Phys. Soc. Jpn.* **7**(1), 5–11 (1952).
- <sup>21</sup>G. Shirane, K. Suzuki, and A. Takeda, "Phase transitions in solid solutions of lead zirconate and lead titanate: II," *J. Phys. Soc. Jpn.* **7**(1), 12–18 (1952).
- <sup>22</sup>I. Ross, "Semiconductive translating device," U.S. patent 2791760A (07 May 1957), see <https://insight.rpxcorp.com/patent/US2791760A>.
- <sup>23</sup>T. P. Ma and J.-P. Han, "Why is nonvolatile ferroelectric memory field-effect transistor still elusive?," *IEEE Electron Device Lett.* **23**, 386–388 (2002).
- <sup>24</sup>D. Bonduant, "Ferroelectric RAM memory family for critical data storage," *Ferroelectrics* **112**, 273–282 (1990).
- <sup>25</sup>C. A.-P. de Araujo, J. D. Cuchiaro, L. D. McMillan *et al.*, "Fatigue-free ferroelectric capacitors with platinum electrodes," *Nature* **374**, 627–629 (1995).
- <sup>26</sup>S. B. Desu, "Minimization of fatigue in ferroelectric films," *Phys. Status Solidi A* **151**, 467–480 (1995).
- <sup>27</sup>C.-U. Pinnow and T. Mikolajick, "Material aspects in emerging nonvolatile memories," *J. Electrochem. Soc.* **151**(6), K13–K19 (2004).
- <sup>28</sup>H. P. McAdams, R. Acklin, T. Blake, X.-H. Du, J. Eliason, J. Fong, W. F. Kraus, D. Liu, S. Madan, T. Moise, S. Natarajan, N. Qian, Y. Qiu, K. A. Remack, J. Rodriguez, J. Roscher, A. Seshadri, and S. R. Summerfelt, "A 64-Mb embedded FRAM utilizing a 130-nm 5LM Cu/FSG logic process," *IEEE J. Solid-State Circuits* **39**, 667–677 (2004).



- <sup>29</sup>J.-M. Koo, B.-S. Seo, S. Kim, S. Shin, J.-H. Lee, H. Baik, J.-H. Lee, J. Lee, B.-J. Bae, J.-E. Lim, D.-C. Yoo, S.-O. Park, H.-S. Kim, H. Han, S. Baik, J.-Y. Choi, Y. J. Park, and Y. Park, "Fabrication of 3D trench PZT capacitors for 256Mbit FRAM device application," *IEDM Technol. Digest* **2005**, 340–343 (2005).
- <sup>30</sup>S. Sakai and R. Ilangoan, "Metal-ferroelectric-insulator-semiconductor memory FET with long retention and high endurance," *IEEE Electron Device Lett.* **25**, 369–371 (2004).
- <sup>31</sup>L. Esaki, R. B. Laibowitz, and P. J. Stiles, "Polar switch," *IBM Tech. Discl. Bull.* **13**, 2161 (1971).
- <sup>32</sup>E. Y. Tsymlal and H. Kohlstedt, "Tunneling across a ferroelectric," *Science* **313**(5784), 181–183 (2006).
- <sup>33</sup>A. Gruverman, D. Wu, H. Lu, Y. Wang, H. W. Jang, C. M. Folkman, M. Ye. Zhuravlev, D. Felker, M. Rzechowski, C.-B. Eom, and E. Y. Tsymlal, "Tunneling electroresistance effect in ferroelectric tunnel junctions at the nanoscale," *Nano Lett.* **9**(10), 3539–3543 (2009).
- <sup>34</sup>A. Tsukazaki, "A platform for making and transferring oxide films," *Nature* **578**, 41–42 (2020).
- <sup>35</sup>H. S. Kum *et al.*, "Heterogeneous integration of single-crystalline complex-oxide membranes," *Nature* **578**, 75–81 (2020).
- <sup>36</sup>T. S. Böscke, J. Müller, D. Bräuhäus, U. Schröder, and U. Böttger, "Ferroelectricity in hafnium oxide: CMOS compatible ferroelectric field effect transistors," in *International Electron Devices Meeting* (IEEE, 2011), pp. 24.5.1–24.5.4.
- <sup>37</sup>U. Schroeder, E. Yurchuk, J. Müller, D. Martin, T. Schenk, P. Polakowski, C. Adelman, M. I. Popovici, S. V. Kalinin, and T. Mikolajick, "Impact of different dopants on the switching properties of ferroelectric hafnium oxide," *Jpn. J. Appl. Phys.* **53**(8S1), 08LE02 (2014).
- <sup>38</sup>P. Polakowski, S. Riedel, W. Weinreich, M. Rudolf, J. Sundqvist, K. Seidel, and J. Müller, "Ferroelectric deep trench capacitors based on Al:HfO<sub>2</sub> for 3D nonvolatile memory applications," in *IEEE International Memory Workshop (IMW)* (IEEE, 2014), pp. 1–4.
- <sup>39</sup>J. Okuno, T. Kunihiro, K. Konishi, H. Maemura, Y. Shuto, S. F. M. Materano, T. Ali, K. Kuehnel, K. Seidel, U. Schroeder, T. Mikolajick, M. Tsukamoto, and T. Umebayashi, "SoC compatible 1T1C FeRAM memory array based on ferroelectric Hf<sub>0.5</sub>Zr<sub>0.5</sub>O<sub>2</sub>," *VLSI Technol.* **2020**, 1–2 (2020).
- <sup>40</sup>S. Fujii, Y. Kamimuta, T. Ino, Y. Nakasaki, R. Takaishi, and M. Saitoh, "First demonstration and performance improvement of ferroelectric HfO<sub>2</sub>-based resistive switch with low operation current and intrinsic diode property," in *IEEE Symposium on VLSI Technology* (IEEE, 2016), pp. 1–2.
- <sup>41</sup>B. Max, M. Hoffmann, S. Slesazek, and T. Mikolajick, "Ferroelectric tunnel junctions based on ferroelectric-dielectric Hf<sub>0.5</sub>Zr<sub>0.5</sub>O<sub>2</sub>/Al<sub>2</sub>O<sub>3</sub> capacitor stacks," in *48th European Solid-State Device Research Conference (ESSDERC)* (IEEE, 2018), pp. 142–145.
- <sup>42</sup>S. Salahuddin and S. Datta, "Use of negative capacitance to provide voltage amplification for low power nanoscale devices," *Nano Lett.* **8**(2), 405–410 (2008).
- <sup>43</sup>J. A. Kittl, B. Obradovic, D. Reddy, T. Rakshit, R. M. Hatcher, and M. S. Rodder, "On the validity and applicability of models of negative capacitance and implications for MOS applications," *Appl. Phys. Lett.* **113**(4), 042904 (2018).
- <sup>44</sup>M. Hoffmann, S. Slesazek, U. Schroeder, and T. Mikolajick, "What's next for negative capacitance electronics?," *Nat. Electron.* **3**, 504–506 (2020).
- <sup>45</sup>K. D. Budd, S. Dey, and D. Payne, "Sol-gel processing of PbTiO<sub>3</sub>, PbZrO<sub>3</sub>, PZT, and PLZT thin films," in *British Ceramic Proceedings* (British Ceramic Society, 1985).
- <sup>46</sup>J. Wang, J. Neaton, H. Zheng, V. Nagarajan, S. Ogale, B. Liu, D. Viehland, V. Vaithyanathan, D. Schlom, and U. Waghmare, "Epitaxial BiFeO<sub>3</sub> multiferroic thin film heterostructures," *Science* **299**(5613), 1719–1722 (2003).
- <sup>47</sup>K. Y. Yun, D. Ricinchi, T. Kanashima, M. Noda, and M. Okuyama, "Giant ferroelectric polarization beyond 150  $\mu\text{C}/\text{cm}^2$  in BiFeO<sub>3</sub> thin film," *Jpn. J. Appl. Phys.* **43**(5A), L647 (2004).
- <sup>48</sup>T. Choi, S. Lee, Y. J. Choi, V. Kyrushin, and S.-W. Cheong, "Switchable ferroelectric diode and photovoltaic effect in BiFeO<sub>3</sub>," *Science* **324**(5923), 63–66 (2009).
- <sup>49</sup>M. H. Park, Y. H. Lee, H. J. Kim, Y. J. Kim, T. Moon, K. D. Kim, J. Müller, A. Kersch, U. Schroeder, T. Mikolajick, and C. S. Hwang, "Ferroelectricity and antiferroelectricity of doped thin HfO<sub>2</sub>-based films," *Adv. Mater.* **27**, 1811–1831 (2015).
- <sup>50</sup>D. Martin, J. Müller, T. Schenk, T. M. Arruda, A. Kumar, E. Strelcov, E. Yurchuk, S. Müller, D. Pohl, U. Schröder, S. V. Kalinin, and T. Mikolajick, "Ferroelectricity in Si-doped HfO<sub>2</sub> revealed: A binary lead-free ferroelectric," *Adv. Mater.* **26**, 8198–8202 (2014).
- <sup>51</sup>S. Mueller, J. Mueller, A. Singh, S. Riedel, J. Sundqvist, U. Schroeder, and T. Mikolajick, "Incipient ferroelectricity in Al-doped HfO<sub>2</sub> thin films," *Adv. Funct. Mater.* **22**, 2412–2417 (2012).
- <sup>52</sup>J. Müller, T. S. Böscke, U. Schröder, S. Mueller, D. Bräuhäus, U. Böttger, L. Frey, and T. Mikolajick, "Ferroelectricity in simple binary ZrO<sub>2</sub> and HfO<sub>2</sub>," *Nano Lett.* **12**(8), 4318–4323 (2012).
- <sup>53</sup>S. Starschich and U. Boettger, "An extensive study of the influence of dopants on the ferroelectric properties of HfO<sub>2</sub>," *J. Mater. Chem. C* **5**, 333–338 (2017).
- <sup>54</sup>M. H. H. Park, H. J. Kim, Y. J. Kim, W. Lee, T. Moon, and C. S. Hwang, "Evolution of phases and ferroelectric properties of thin Hf<sub>0.5</sub>Zr<sub>0.5</sub>O<sub>2</sub> films according to the thickness and annealing temperature," *Appl. Phys. Lett.* **102**(24), 242905 (2013).
- <sup>55</sup>L. Xu, T. Nishimura, S. Shibayama, T. Yajima, S. Migita, and A. Toriumi, "Kinetic pathway of the ferroelectric phase formation in doped HfO<sub>2</sub> films," *J. Appl. Phys.* **122**(12), 124104 (2017).
- <sup>56</sup>Y. Wei, P. Nukala, M. Salverda, S. Matzen, H. J. Zhao, J. Momand, A. S. Everhardt, G. Agnus, G. R. Blake, P. Lecoeur, B. J. Kooi, J. Iniguez, B. Dkhil, and B. Noheda, "A rhombohedral ferroelectric phase in epitaxially strained Hf<sub>0.5</sub>Zr<sub>0.5</sub>O<sub>2</sub> thin films," *Nat. Mater.* **17**(12), 1095 (2018).
- <sup>57</sup>X. Sang, E. D. Grimley, T. Schenk, U. Schroeder, and J. M. LeBeau, "On the structural origins of ferroelectricity in HfO<sub>2</sub> thin films," *Appl. Phys. Lett.* **106**, 162905 (2015).
- <sup>58</sup>R. Materlik, C. Kunneth, and A. Kersch, "The origin of ferroelectricity in Hf<sub>1-x</sub>Zr<sub>x</sub>O<sub>2</sub>: A computational investigation and a surface energy model," *J. Appl. Phys.* **117**(13), 134109 (2015).
- <sup>59</sup>M. H. Park, D. H. Lee, K. Yang, J.-Y. Park, G. T. Yu, H. W. Park, M. M. Materano, T. Mittmann, P. D. Lomenzo, and T. Mikolajick, "Review of defect chemistry in fluorite-structure ferroelectrics for future electronic devices," *J. Mater. Chem. C* **8**, 10526–10550 (2020).
- <sup>60</sup>H. J. Kim, M. H. Park, Y. J. Kim, Y. H. Lee, W. Jeon, T. Gwon, T. Moon, K. D. Kim, and C. S. Hwang, "Grain size engineering for ferroelectric Hf<sub>0.5</sub>Zr<sub>0.5</sub>O<sub>2</sub> films by an insertion of Al<sub>2</sub>O<sub>3</sub> interlayer," *Appl. Phys. Lett.* **105**(19), 192903 (2014).
- <sup>61</sup>K. D. Kim, M. H. Park, H. J. Kim, Y. J. Kim, T. Moon, Y. H. Lee, S. D. Hyun, T. Gwon, and C. S. Hwang, "Ferroelectricity in undoped-HfO<sub>2</sub> thin films induced by deposition temperature control during atomic layer deposition," *J. Mater. Chem. C* **4**(28), 6864–6872 (2016).
- <sup>62</sup>M. H. Park, C.-C. Chung, T. Schenk, C. Richter, M. Hoffmann, S. Wirth, J. L. Jones, T. Mikolajick, and U. Schroeder, "Origin of temperature-dependent ferroelectricity in Si-doped HfO<sub>2</sub>," *Adv. Electron. Mater.* **4**, 1700489 (2018).
- <sup>63</sup>M. H. Park, C.-C. Chung, T. Schenk, C. Richter, K. Opsomer, C. Detavernier, C. Adelman, J. L. Jones, T. Mikolajick, and U. Schroeder, "Effect of annealing ferroelectric HfO<sub>2</sub> thin films: In situ, high temperature x-ray diffraction," *Adv. Electron. Mater.* **4**(7), 1800091 (2018).
- <sup>64</sup>M. H. Park, T. Schenk, and U. Schroeder, "Dopants in atomic layer deposited HfO<sub>2</sub> thin films," in *Ferroelectricity in Doped Hafnium Oxide: Materials, Properties and Devices* (Elsevier, 2019), pp. 49–74.
- <sup>65</sup>M. H. Park, T. Schenk, C. M. Fancher, E. D. Grimley, C. Zhou, C. Richter, J. M. LeBeau, J. L. Jones, T. Mikolajick, and U. Schroeder, "A comprehensive study on the structural evolution of HfO<sub>2</sub> thin films doped with various dopants," *J. Mater. Chem. C* **5**(19), 4677–4690 (2017).
- <sup>66</sup>T. Mimura, T. Shimizu, H. Uchida, O. Sakata, and H. Funakubo, "Thickness-dependent crystal structure and electric properties of epitaxial ferroelectric Y<sub>2</sub>O<sub>3</sub>-HfO<sub>2</sub> films," *Appl. Phys. Lett.* **113**(10), 102901 (2018).

- <sup>67</sup>H. F. Kay and J. W. Dunn, "Thickness dependence of the nucleation field of triglycine sulphate," *Philos. Mag.* **7**(84), 2027–2034 (1962).
- <sup>68</sup>M. H. Park, Y. H. Lee, H. J. Kim, Y. J. Kim, T. Moon, K. D. Kim, S. D. Hyun, and C. S. Hwang, "Morphotropic phase boundary of  $\text{Hf}_{1-x}\text{Zr}_x\text{O}_2$  thin films for dynamic random access memories," *ACS Appl. Mater. Interfaces* **10**(49), 42666–42673 (2018).
- <sup>69</sup>D. Zhou, J. Xu, Q. Li, Y. Guan, F. Cao, X. Dong, J. Muller, T. Schenk, and U. Schroder, "Wake-up effects in Si-doped hafnium oxide ferroelectric thin films," *Appl. Phys. Lett.* **103**(19), 192904 (2013).
- <sup>70</sup>M. Pešić, F. P. G. Fengler, L. Larcher, A. Padovani, T. Schenk, E. D. Grimley, X. Sang, J. M. LeBeau, S. Slesazek, U. Schroeder, and T. Mikolajick, "Physical mechanisms behind the field-cycling behavior of  $\text{HfO}_2$ -based ferroelectric capacitors," *Adv. Funct. Mater.* **26**(25), 4601–4612 (2016).
- <sup>71</sup>H. J. Kim, M. H. Park, Y. J. Kim, Y. H. Lee, T. Moon, K. D. Kim, S. D. Hyun, and C. S. Hwang, "A study on the wake-up effect of ferroelectric  $\text{Hf}_{0.5}\text{Zr}_{0.5}\text{O}_2$  films by pulse-switching measurement," *Nanoscale* **8**(3), 1383–1389 (2016).
- <sup>72</sup>E. D. Grimley, T. Schenk, X. Sang, M. Pesic, U. Schroeder, T. Mikolajick, and J. M. LeBeau, "Structural changes underlying field-cycling phenomena in ferroelectric  $\text{HfO}_2$  thin films," *Adv. Electron. Mater.* **2**(9), 1600173 (2016).
- <sup>73</sup>M. H. Park, T. Schenk, S. Starschich, C. M. Fancher, H. J. Kim, U. Böttger, C. S. Hwang, A. Toriumi, X. Tian, and U. Schroeder, "Effect of surface/interface energy and stress on the ferroelectric properties," in *Ferroelectricity in Doped Hafnium Oxide: Materials, Properties and Devices* (Elsevier, 2019), pp. 145–172.
- <sup>74</sup>M. H. Park, Y. H. Lee, H. J. Kim, T. Schenk, W. Lee, K. D. Kim, F. P. G. Fengler, T. Mikolajick, U. Schroeder, and C. S. Hwang, "Surface and grain boundary energy as the key enabler of ferroelectricity in nanoscale hafnia-zirconia: A comparison of model and experiment," *Nanoscale* **9**, 9973–9986 (2017).
- <sup>75</sup>S. Zhang, D. Holec, W. Y. Fu, C. J. Humphreys, and M. A. Moram, "Tunable optoelectronic and ferroelectric properties in Sc-based III-nitrides," *J. Appl. Phys.* **114**, 133510 (2013).
- <sup>76</sup>F. Tasnadi, B. Alling, C. Höglund, G. Wingqvist, J. Birch, L. Hultman, and I. A. Abrikosov, "Origin of the anomalous piezoelectric response in wurtzite," *Phys. Rev. Lett.* **104**, 137601 (2010).
- <sup>77</sup>H. Moriwake, A. Konishi, T. Ogawa, K. Fujimura, C. A. J. Fisher, A. Kuwabara, T. Shimizu, S. Yasui, and M. Itoh, "Mechanism of polarization switching in wurtzite-structured zinc oxide thin films," *Appl. Phys. Lett.* **104**, 242909 (2014).
- <sup>78</sup>N. Takeuchi, "First-principles calculations of the ground-state properties and stability of ScN," *Phys. Rev. B* **65**, 045204 (2002).
- <sup>79</sup>N. Farrer and L. Bellaiche, "Properties of hexagonal ScN versus wurtzite GaN and InN," *Phys. Rev. B* **66**, 201203 (2002).
- <sup>80</sup>M. Akiyama, T. Kamohara, K. Kano, A. Teshigahara, Y. Takeuchi, and N. Kawahara, "Enhancement of piezoelectric response in scandium aluminum nitride alloy thin films prepared by dual reactive cosputtering," *Adv. Mater.* **21**(5), 593 (2009).
- <sup>81</sup>R. Aigner and G. Fattinger, "3G—4G—5G: How Baw filter technology enables a connected world," in *20th International Conference on Solid-State Sensors, Actuators Microsystems, Eurosensors* (American Elements, 2019), p. 523.
- <sup>82</sup>M. Akiyama, K. Umeda, A. Honda, and T. Nagase, "Influence of scandium concentration on power generation figure of merit of scandium aluminum nitride thin films," *Appl. Phys. Lett.* **102**, 021915 (2013).
- <sup>83</sup>T. Yanagitani and M. Suzuki, "Electromechanical coupling and gigahertz elastic properties of ScAlN films near phase boundary," *Appl. Phys. Lett.* **105**, 122907 (2014).
- <sup>84</sup>S. Fichtner, N. Wolff, G. Krishnamurthy, A. Petraru, S. Bohse, F. Lofink, S. Chennitiz, H. Kohlstedt, L. Kienle, and B. Wagner, "Identifying and overcoming the interface originating c-axis instability in highly Sc enhanced AlN for piezoelectric micro-electromechanical systems," *J. Appl. Phys.* **122**, 035301 (2017).
- <sup>85</sup>M. Joseph, H. Tabata, and T. Kawai, "Ferroelectric behavior of Li-doped ZnO thin films on Si(100) by pulsed laser deposition," *Appl. Phys. Lett.* **74**, 2534 (1999).
- <sup>86</sup>Y. C. Yang, C. Song, X. H. Wang, F. Zeng, and F. Pan, "Giant piezoelectric d33 coefficient in ferroelectric vanadium doped ZnO films," *Appl. Phys. Lett.* **92**, 012907 (2008).
- <sup>87</sup>S. Fichtner, D. Kaden, F. Lofink, and B. Wagner, "A generic CMOS compatible piezoelectric multilayer actuator approach based on permanent ferroelectric polarization inversion in  $\text{Al}_{1-x}\text{Sc}_x\text{N}$ ," in *20th International Conference On Solid-State Sensors, Actuators Microsystems, Eurosensors* (Web of Science, 2019), p. 289.
- <sup>88</sup>S. Fichtner, G. Schönweger, T.-N. Kreutzer, A. Petraru, H. Kohlstedt, F. Lofink, and B. Wagner, in *Proceedings of ISAF* (IEEE, 2020).
- <sup>89</sup>S. Yasuoka, T. Shimizu, A. Tateyama, M. Uehara, H. Yamada, M. Akiyama, Y. Hiranaga, Y. Cho, and H. Funakubo, "Effects of deposition conditions on the ferroelectric properties of  $(\text{Al}_{1-x}\text{Sc}_x)\text{N}$  thin films," *J. Appl. Phys.* **128**, 114103 (2020).
- <sup>90</sup>S. Fichtner, "Ferroelectricity in AlScN: Switching, imprint and sub-150nm films," in *Proceedings of 2020 IEEE IFCS-ISAF* (IEEE, 2020).
- <sup>91</sup>X. Wang, O. B. X. B. Saadat, X. Lou, R. J. Molnar, T. Palacios, and R. G. Gordon, "Atomic layer deposition of  $\text{Sc}_2\text{O}_3$  for passivating AlGaIn/GaN high electron mobility transistor devices," *Appl. Phys. Lett.* **101**, 232109 (2012).
- <sup>92</sup>S. Huang, Q. Jiang, S. Yang, C. Zhou, and K. J. Chen, "Effective passivation of AlGaIn/GaN HEMTs by ALD-grown AlN thin film," *IEEE Electron Device Lett.* **33**(4), 516–518 (2012).
- <sup>93</sup>V. Tarala, M. Ambartsumov, A. Altkhov, V. Martens, and M. Shevchenko, "Growing c-axis oriented aluminum nitride films by plasma-enhanced atomic layer deposition at low temperatures," *J. Cryst. Growth* **455**, 157–160 (2016).
- <sup>94</sup>V. Rontu, P. Sippola, M. Broas, G. Ross, T. Sajavaara, H. Lipsanen, M. Paulasto-Kröckel, and S. Franssila, "Atomic layer deposition of AlN from  $\text{AlCl}_3$  using  $\text{NH}_3$  and  $\text{Ar}/\text{NH}_3$  plasma," *J. Vac. Sci. Technol. A* **36**, 021508 (2018).
- <sup>95</sup>M. T. Hardy, E. N. Jin, N. Nepal, D. S. Katzer, B. P. Downey, V. J. Gokhale, D. F. Storm, and D. J. Meyer, "Control of phase purity in high scandium fraction heteroepitaxial ScAlN grown by molecular beam epitaxy," *Appl. Phys. Express* **13**(6), 065509 (2020).
- <sup>96</sup>S. Leone, J. Ligl, C. Manz, L. Kirste, T. Fuchs, H. Menner, M. Prescher, J. Wiegert, A. Zukauskaitė, R. Quay, and O. Ambacher, "Metal-organic chemical vapor deposition of aluminum scandium nitride," *Phys. Status Solidi RRL* **14**(1), 1900535 (2020).
- <sup>97</sup>A. J. Green *et al.*, "ScAlN/GaN high-electron-mobility transistors with 2.4-A/mm current density and 0.67-S/mm transconductance," *IEEE Electron Device Lett.* **40**(7), 1056–1059 (2019).
- <sup>98</sup>J. Ligl, S. Leone, C. Manz, L. Kirste, P. Doering, T. Fuchs, M. Prescher, and O. Ambacher, "Metalorganic chemical vapor phase deposition of AlScN/GaN heterostructures," *J. Appl. Phys.* **127**, 195704 (2020).
- <sup>99</sup>K. D. Budd, S. Dey, and D. Payne, "Sol-gel processing of  $\text{PbTiO}_3$ ,  $\text{PbZrO}_3$ , PZT, and PLZT thin films," *British Ceram. Proc.* **36**, 107–121 (1985), see [https://www.researchgate.net/publication/282383364\\_Sol-Gel\\_Processing\\_of\\_PbTiO3\\_PbZrO3\\_PZT\\_and\\_PLZT\\_Thin\\_Films](https://www.researchgate.net/publication/282383364_Sol-Gel_Processing_of_PbTiO3_PbZrO3_PZT_and_PLZT_Thin_Films).
- <sup>100</sup>D. Wang, J. Zheng, P. Musavigharavi, W. Zhu, A. Foucher, S. Trolier-McKinstry, E. Stach, and R. Olsson III, "Ferroelectric switching in sub-20 nm aluminum scandium nitride thin films," *Electron Device Lett.* **41**(12), 1774–1777 (2020).
- <sup>101</sup>M. H. Park, T. Schenk, and U. Schröder, "Dopants in atomic layer deposited  $\text{HfO}_2$  thin films," in *Ferroelectricity in Doped  $\text{HfO}_2$ : Material Properties and Devices* (Elsevier, 2019), pp. 49–74.
- <sup>102</sup>M. H. Park, H. J. Kim, K. D. Kim, Y. H. Lee, S. D. Hyun, and C. S. Hwang, "Impact of Zr content in atomic layer deposited  $\text{Hf}_{1-x}\text{Zr}_x\text{O}_2$  thin films," in *Ferroelectricity in Doped  $\text{HfO}_2$ : Material Properties and Devices* (Elsevier, 2019).
- <sup>103</sup>M. H. Park, T. Schenk, and U. Schroeder, "Impact of Zr Content in Atomic Layer Deposited  $\text{Hf}_{1-x}\text{Zr}_x\text{O}_2$  Thin Films," in *Ferroelectricity in Doped Hafnium Oxide: Materials, Properties and Devices* (Elsevier, 2019), pp. 75–101.
- <sup>104</sup>A. Toriumi, M. Materano, M. Hoffmann, T. Mikolajick, and U. Schroeder, "On the polarization reversal kinetics in ferroelectric  $\text{HfO}_2$ " (unpublished).
- <sup>105</sup>P. D. Lomenzo *et al.*, "Ferroelectric  $\text{Hf}_{1-x}\text{Zr}_x\text{O}_2$  memories: Device reliability and depolarization fields," in *19th Non-Volatile Memory Technology Symposium (NVMTS)* (IEEE, 2019), pp. 1–8.

- <sup>106</sup>J. Rodriguez *et al.*, “Reliability of ferroelectric random access memory embedded within 130nm CMOS,” in *IEEE International Reliability Physics Symposium* (IEEE, 2010), pp. 750–758.
- <sup>107</sup>J. Muller, T. Boscke, S. Muller, E. Y. P. Polakowski, J. Paul, D. Martin, T. Schenk, K. Khullar, A. Kersch, W. Weinreich, S. Riedel, K. Seidel, A. Kumar, T. Arruda, S. Kalinin, T. Schlosser, R. Boschke, R. V. Bentum, U. Schroder, and T. Mikolajick, “Ferroelectric hafnium oxide: A CMOS-compatible and highly scalable approach to future ferroelectric memories,” in *IEEE International Electron Devices Meeting (IEDM)* (IEEE, 2013), pp. 10.8.1–10.8.4.
- <sup>108</sup>S. Dünkler, M. Trentzsch, R. Richter, P. Moll, C. Fuchs, O. Gehring, M. Majer, S. Witte, B. Müller, T. Melde, H. Mulaosmanovic, S. Slesazek, S. Müller, J. Ocker, M. Noack, D.-A. Löhr, P. Polakowski, J. Müller, T. Mikolajick, and J. Höntsch, “A FeFET based super-low-power ultra-fast embedded NVM technology for 22nm FDSOI and beyond,” in *IEEE International Electron Devices Meeting (IEDM)* (IEEE, 2017), pp. 19.7.1–19.7.4.
- <sup>109</sup>E. Yurchuk, J. Müller, S. Müller, J. Paul, M. Pešić, R. V. Bentum, U. Schroeder, and T. Mikolajick, “Charge-trapping phenomena in HfO<sub>2</sub>-based FeFET-type nonvolatile memories,” *IEEE Trans. Electron Devices* **63**(9), 3501–3507 (2016), see <https://ieeexplore.ieee.org/document/7519093>.
- <sup>110</sup>J. Muller, P. Polakowski, S. Muller, H. Mulaosmanovic, J. Ocker, T. Mikolajick, S. Slesazek, S. Flachowsky, and M. Trentzsch, “High endurance strategies for hafnium oxide based ferroelectric field effect transistor,” in *Non-Volatile Memory Technology Symposium (NVMTS)* (IEEE, 2016), pp. 1–7.
- <sup>111</sup>W. Hamouda, A. Pancotti, C. Lubin, L. Tortech, C. Richter, T. Mikolajick, U. Schroeder, and N. Barrett, “Physical chemistry of the TiN/Hf<sub>0.5</sub>Zr<sub>0.5</sub>O<sub>2</sub> interface,” *J. Appl. Phys.* **127**, 064105 (2020).
- <sup>112</sup>H. Mulaosmanovic, J. Ocker, S. Mueller, U. Schroeder, J. Mueller, P. Polakowski, S. Flachowsky, R. Bentum, T. Mikolajick, and S. Slesazek, “Switching kinetics in nanoscale hafnium oxide based ferroelectric field-effect transistors,” *ACS Appl. Mater. Interfaces* **9**(4), 3792–3798 (2017).
- <sup>113</sup>A. G. Chernikova *et al.*, “Improved ferroelectric switching endurance of La-doped Hf<sub>0.5</sub>Zr<sub>0.5</sub>O<sub>2</sub> thin films,” *ACS Appl. Mater. Interfaces* **10**(3), 2701–2708 (2018).
- <sup>114</sup>S. Slesazek, U. Schroeder, and T. Mikolajick, “Embedding hafnium oxide based FeFETs in the memory landscape,” in *International Conference on IC Design & Technology (ICIDT)* (IEEE, 2018), pp. 121–124.
- <sup>115</sup>T. Francois *et al.*, “Demonstration of BEOL-compatible ferroelectric Hf<sub>0.5</sub>Zr<sub>0.5</sub>O<sub>2</sub> scaled FeRAM co-integrated with 130nm CMOS for embedded NVM applications,” in *IEEE International Electron Devices Meeting (IEDM)* (IEEE, 2019), pp. 1–4.
- <sup>116</sup>S. Slesazek, V. Havel, E. Breyer, H. Mulaosmanovic, M. Hoffmann, B. Max, S. Duenkel, and T. Mikolajick, “Uniting the trinity of ferroelectric HfO<sub>2</sub> memory devices in a single memory cell,” in *IEEE International Memory Workshop (IMW)* (IEEE, 2019), pp. 1–4.
- <sup>117</sup>M. Trentzsch, S. Flachowsky, R. Richter, J. Paul, B. Reimer, D. Utes, S. Jansen, H. Mulaosmanovic, S. Müller, S. Slesazek, J. Ocker, M. Noack, J. Müller, P. Polakowski, J. Schreiter, S. Beyer, T. Mikolajick, and B. Rice, “A 28nm HKMG super low power embedded NVM technology based on ferroelectric FETs,” in *IEEE International Electron Devices Meeting (IEDM)* (IEEE, 2016), pp. 11.5.1–11.5.4.
- <sup>118</sup>S. Beyer *et al.*, “FeFET: A versatile CMOS compatible device with game-changing potential,” in *IEEE International Memory Workshop (IMW)* (IEEE, 2020), pp. 1–4.
- <sup>119</sup>E. Yurchuk, S. Mueller, D. Martin, S. Slesazek, U. Schroeder, T. Mikolajick, J. Müller, J. Paul, R. S. J. Hoffmann, T. Schlösser, R. Boschke, R. van Bentum, and M. Trentzsch, “Origin of the endurance degradation in the novel HfO<sub>2</sub>-based 1T ferroelectric non-volatile memories,” in *IEEE International Reliability Physics Symposium* (IEEE, 2014), pp. 2E.5.1–2E.5.5.
- <sup>120</sup>K. Chatterjee *et al.*, “Self-aligned, gate last, FDSOI, ferroelectric gate memory device with 5.5-nm Hf<sub>0.8</sub>Zr<sub>0.2</sub>O<sub>2</sub>, high endurance and breakdown recovery,” *IEEE Electron Device Lett.* **38**(10), 1379–1382 (2017).
- <sup>121</sup>C. Zacharakis *et al.*, “Very large remanent polarization in ferroelectric Hf<sub>1-x</sub>Zr<sub>x</sub>O<sub>2</sub> grown on Ge substrates by plasma assisted atomic oxygen deposition,” *Appl. Phys. Lett.* **114**(11), 112901 (2019).
- <sup>122</sup>F. Mo *et al.*, “Experimental demonstration of ferroelectric HfO<sub>2</sub> FET with ultrathin-body IGZO for high-density and low-power memory application,” in *Symposium on VLSI Technology* (IEEE, 2019), pp. 1–4.
- <sup>123</sup>S. Mueller *et al.*, “From MFM capacitors toward ferroelectric transistors: Endurance and disturb characteristics of HfO<sub>2</sub>-based FeFET devices,” *IEEE Trans. Electron Devices* **60**(12), 4199–4205 (2013).
- <sup>124</sup>A. Sharma and K. Roy, “1T non-volatile memory design using sub-10nm ferroelectric FETs,” *IEEE Electron Device Lett.* **39**(3), 359–362 (2018).
- <sup>125</sup>H. Mulaosmanovic, S. Slesazek, J. Ocker, M. Pesic, S. Muller, S. Flachowsky, J. Müller, P. Polakowski, J. Paul, S. Jansen, S. Kolodinski, C. Richter, S. Piontek, T. Schenk, A. Kersch, C. Kuneth, R. V. Bentum, U. Schroder, and T. Mikolajick, “Evidence of single domain switching in hafnium oxide based FeFETs: Enabler for multi-level FeFET memory cells,” in *IEEE International Electron Devices Meeting (IEDM)* (IEEE, 2015), pp. 26.8.1–26.8.3.
- <sup>126</sup>H. Mulaosmanovic, E. T. Breyer, T. Mikolajick, and S. Slesazek, “Ferroelectric FETs with 20-nm-thick HfO<sub>2</sub> layer for large memory window and high performance,” *IEEE Trans. Electron Devices* **66**(9), 3828–3833 (2019).
- <sup>127</sup>K. Florent, S. Lavizzari, L. Di Piazza, M. Popovici, V. E., P. G. G. Groeseneken, and J. Van Houdt, “First demonstration of vertically stacked ferroelectric Al doped HfO<sub>2</sub> devices for NAND applications,” in *Symposium on VLSI Technology* (IEEE, 2017), pp. T158–T159.
- <sup>128</sup>M. Y. Zhuravlev, R. F. Sabirianov, S. S. Jaswal, and E. Y. Tsybmal, “Giant electroresistance in ferroelectric tunnel junctions,” *Phys. Rev. Lett.* **94**, 246802 (2005).
- <sup>129</sup>H. Kohlstedt, N. A. Pertsev, J. Rodríguez Contreras, and R. Waser, “Theoretical current-voltage characteristics of ferroelectric tunnel junctions,” *Phys. Rev. B* **72**, 125341 (2005).
- <sup>130</sup>M. Y. Zhuravlev, Y. Wang, S. Maekawa, and E. Y. Tsybmal, “Tunnelling electroresistance in ferroelectric tunnel junctions with a composite barrier,” *Appl. Phys. Lett.* **95**, 052902 (2009).
- <sup>131</sup>Z. J. Ma, T. J. Zhang, R. K. Pan, M. G. Duan, and M. He, “Optimal dielectric thickness for ferroelectric tunnel junctions with a composite barrier,” *J. Appl. Phys.* **111**, 074311 (2012).
- <sup>132</sup>B. Max, M. Hoffmann, S. Slesazek, and T. Mikolajick, “Direct correlation of ferroelectric properties and memory characteristics in ferroelectric tunnel junctions,” *IEEE J. Electron Devices Soc.* **7**, 1175 (2019).
- <sup>133</sup>S. Slesazek and T. Mikolajick, “Nanoscale resistive switching memory devices: A review,” *Nanotechnology* **30**(35), 352003 (2019).
- <sup>134</sup>E. J. Fuller, S. T. Keene, A. Melianas, Z. Wang, S. Agarwal, Y. Yiyang Li, Y. Tuchman, C. D. James, M. J. Marinella, J. J. Yang, A. Salleo, and A. A. Talin, “Parallel programming of an ionic floating-gate memory array for scalable neuromorphic computing,” *Science* **364**(6440), 570–574 (2019), see <https://science.sciencemag.org/content/364/6440/570>.
- <sup>135</sup>B. Max, M. Hoffmann, H. Mulaosmanovic, S. Slesazek, and T. Mikolajick, “Hafnia-based double layer ferroelectric tunnel junctions as artificial synapses for neuromorphic computing,” *ACS Appl. Electron. Mater.* **2**(12), 4023–4033 (2020).
- <sup>136</sup>E. T. Breyer, H. Mulaosmanovic, T. Mikolajick, and S. Slesazek, “Reconfigurable NAND/NOR logic gates in 28nm HKMG and 22nm FD-SOI FeFET technology,” in *IEEE International Electron Devices Meeting (IEDM)* (IEEE, 2017), pp. 28.5.1–28.5.4.
- <sup>137</sup>E. T. Breyer, H. Mulaosmanovic, S. Slesazek, and T. Mikolajick, “Demonstration of versatile nonvolatile logic gates in 28 nm HKMG FeFET technology,” in *IEEE International Symposium on Circuits and Systems (ISCAS)* (IEEE, 2018), pp. 1–5.
- <sup>138</sup>E. T. Breyer, H. Mulaosmanovic, S. Slesazek, and T. Mikolajick, “Perspective on ferroelectric, hafnium oxide based transistors for digital beyond von-Neumann computing,” *Appl. Phys. Lett.* **118**, 050501 (2021).
- <sup>139</sup>R. Berdan *et al.*, “Low-power linear computation using nonlinear ferroelectric tunnel junction memristors,” *Nat. Electron.* **3**, 259–266 (2020).
- <sup>140</sup>M. Jerry *et al.*, “Ferroelectric FET analog synapse for acceleration of deep neural network training,” in *IEEE International Electron Devices Meeting (IEDM)* (IEEE, 2017), pp. 6.2.1–6.2.4.

- <sup>141</sup>P. Wang and S. Yu, "Ferroelectric devices and circuits for neuro-inspired computing," *MRS Commun.* **10**(4), 538–548 (2020).
- <sup>142</sup>H. Mulaosmanovic, J. Ocker, S. Müller, M. Noack, J. Müller, P. Polakowski, T. Mikolajick, and S. Slesazek, "Novel ferroelectric FET based synapse for neuromorphic systems," in *Symposium on VLSI Technology* (IEEE, 2017), pp. T176–T177.
- <sup>143</sup>H. Ryu *et al.*, "Ferroelectric tunneling junctions based on aluminum oxide/zirconium-doped hafnium oxide for neuromorphic computing," *Sci. Rep.* **9**, 20383 (2019).
- <sup>144</sup>B. Max, M. Hoffmann, H. Mulaosmanovic, S. Slesazek, and T. Mikolajick, "Hafnia-based double-layer ferroelectric tunnel junctions as artificial synapses for neuromorphic computing," *ACS Appl. Electron. Mater.* **2**(12), 4023–4033 (2020).
- <sup>145</sup>H. Mulaosmanovic, E. Chicca, M. Bertele, T. Mikolajick, and S. Slesazek, "Mimicking biological neurons with a nanoscale ferroelectric transistor," *Nanoscale* **10**(46), 21755–21763 (2018).
- <sup>146</sup>T. N. Theis and P. M. Solomon, "It's time to reinvent the transistor!," *Science* **327**, 1600–1601 (2010).
- <sup>147</sup>V. V. Zhirnov and R. K. Cavin, "Negative capacitance to the rescue?," *Nat. Nanotechnol.* **3**, 77–78 (2008).
- <sup>148</sup>M. Hoffmann, A. I. Khan, C. Serrao, Z. Lu, S. Salahuddin, M. Pešić, S. Slesazek, U. Schroeder, and T. Mikolajick, "Ferroelectric negative capacitance domain dynamics," *J. Appl. Phys.* **123**, 184101 (2018), see <https://www.nature.com/articles/nnano.2008.18>.
- <sup>149</sup>J. Iñiguez, P. Zubko, I. Luk'yanchuk, and A. Cano, "Ferroelectric negative capacitance," *Nat. Rev. Mater.* **4**, 243–256 (2019).
- <sup>150</sup>M. A. Alam, M. Si, and P. D. Ye, "A critical review of recent progress on negative capacitance field-effect transistors," *Appl. Phys. Lett.* **114**, 090401 (2019).
- <sup>151</sup>A. Cano and D. Jiménez, "Multidomain ferroelectricity as a limiting factor for voltage amplification in ferroelectric field-effect transistors," *Appl. Phys. Lett.* **97**, 133509 (2010).
- <sup>152</sup>A. I. Khan, K. Chatterjee, B. Wang *et al.*, "Negative capacitance in a ferroelectric capacitor," *Nat. Mater.* **14**, 182–186 (2015).
- <sup>153</sup>H. Hoffmann, M. Pešić, K. Chatterjee, A. I. S. S. Khan, S. Slesazek, U. Schroeder, and T. Mikolajick, "Direct observation of negative capacitance in polycrystalline ferroelectric HfO<sub>2</sub>," *Adv. Funct. Mater.* **26**, 8643–8649 (2016).
- <sup>154</sup>G. A. Salvatore, A. Rusu, and A. M. Ionescu, "Experimental confirmation of temperature dependent negative capacitance in ferroelectric field effect transistor," *Appl. Phys. Lett.* **100**, 163504 (2012).
- <sup>155</sup>G. Catalan, D. Jiménez, and A. Gruverman, "Negative capacitance detected," *Nat. Mater.* **14**, 137–139 (2015).
- <sup>156</sup>S.-C. Chang, U. E. Avci, D. E. Nikonov, S. Manipatruni, and I. A. Young, "Physical origin of transient negative capacitance in a ferroelectric capacitor," *Phys. Rev. Appl.* **9**, 014010 (2018).
- <sup>157</sup>A. I. Khan, U. Radhakrishna, K. Chatterjee, S. Salahuddin, and D. A. Antoniadis, "Negative capacitance behavior in a leaky ferroelectric," *IEEE Trans. Electron Devices* **63**, 4416–4422 (2016).
- <sup>158</sup>M. Hoffmann, M. Pešić, S. Slesazek, S. Schroeder, and T. Mikolajick, "On the stabilization of ferroelectric negative capacitance in nanoscale devices," *Nanoscale* **10**, 10891–10899 (2018).
- <sup>159</sup>M. Hoffmann, B. Max, T. Mittmann, U. Schroeder, S. Slesazek, and T. Mikolajick, "Demonstration of high-speed hysteresis-free negative capacitance in Ferroelectric Hf<sub>0.5</sub>Zr<sub>0.5</sub>O<sub>2</sub>," in *IEEE International Electron Devices Meeting (IEDM)* (IEEE, 2018), pp. 31.6.1–31.6.4.
- <sup>160</sup>M. Hoffmann, F. G. P. Fengler, M. Herzig, T. M. B. Mittmann, U. Schroeder, R. L. P. Negrea, S. Slesazek, and T. Mikolajick, "Unveiling the double-well energy landscape in a ferroelectric layer," *Nature* **565**, 464–467 (2019).
- <sup>161</sup>K. D. Kim, Y. J. Kim, M. H. Park, H. W. Park, Y. J. Kwon, Y. B. Lee, H. J. Kim, T. Moon, Y. H. Lee, S. D. Hyun, B. S. Kim, and C. S. Hwang, "Transient negative capacitance effect in atomic-layer-deposited Al<sub>2</sub>O<sub>3</sub>/Hf<sub>0.3</sub>Zr<sub>0.7</sub>O<sub>2</sub> bilayer thin film," *Adv. Funct. Mater.* **29**, 1808228 (2019).
- <sup>162</sup>M. Hoffmann, F. G. P. Fengler, B. Max, U. Schroeder, S. Slesazek, and T. Mikolajick, "Negative capacitance for electrostatic supercapacitors," *Adv. Energy Mater.* **9**, 1901154 (2019).
- <sup>163</sup>S. S. Cheema, D. Kwon, N. Shanker, R. dos Reis, and S.-L. E. A. Hsu, "Enhanced ferroelectricity in ultrathin films grown directly on silicon," *Nature* **580**, 478–482 (2020).
- <sup>164</sup>D. Kwon, S. Cheema, N. Shanker, K. Chatterjee, Y.-H. Liao, A. J. Tan, C. Hu, and S. Salahuddin, "Negative capacitance FET With 1.8-nm-thick Zr-doped HfO<sub>2</sub> oxide," *IEEE Electron Device Lett.* **40**, 993–996 (2019).
- <sup>165</sup>Y.-H. Liao, D. Kwon, Y.-K. Lin, A. J. Tan, C. Hu, and S. Salahuddin, "Anomalous beneficial gate-length scaling trend of negative capacitance transistors," *IEEE Electron Device Lett.* **40**, 1860–1863 (2019).
- <sup>166</sup>D. Kwon, S. Cheema, Y.-K. Lin, Y.-H. Liao, K. Chatterjee, A. J. Tan, C. Hu, and S. Salahuddin, "Near threshold capacitance matching in a negative capacitance FET with 1 nm effective oxide thickness gate stack," *IEEE Electron Device Lett.* **41**, 179–182 (2020).
- <sup>167</sup>W. Cao and K. Banerjee, "Is negative capacitance FET a steep-slope logic switch?," *Nat. Commun.* **11**, 196 (2020).
- <sup>168</sup>M. H. Park and C. S. Hwang, "Fluorite-structure antiferroelectrics," *Rep. Prog. Phys.* **82**(12), 124502 (2019).
- <sup>169</sup>S. Pandya, G. Velarde, L. Zhang, and L. W. Martin, "Pyroelectric and electrocaloric effects in ferroelectric silicon-doped hafnium oxide thin films," *Phys. Rev. Mater.* **2**(12), 124405 (2018).
- <sup>170</sup>M. H. Park and C. S. Hwang, "Novel applications of antiferroelectrics and relaxor ferroelectrics: A material's point of view," in *Ferroelectric-Gate Field Effect Transistor Memories: Device Physics and Applications*, 2nd ed., edited by B. E. Park, H. Ishiwara, M. Okuyama, S. Sakai, and S. M. Yoon (Springer, 2020), pp. 295–310.
- <sup>171</sup>M. H. Park, H. J. Kim, Y. J. Kim, T. Moon, K. D. Kim, and C. S. Hwang, "Toward a multifunctional monolithic device based on pyroelectricity and the electrocaloric effect of thin antiferroelectric Hf<sub>x</sub>Zr<sub>1-x</sub>O<sub>2</sub> films," *Nano Energy* **12**, 131–140 (2015).
- <sup>172</sup>M. Hoffmann, U. Schroeder, C. Kuneth, A. Kersch, S. Starschich, U. Bottger, and T. Mikolajick, "Ferroelectric phase transitions in nanoscale HfO<sub>2</sub> films enable giant pyroelectric energy conversion and highly efficient supercapacitors," *Nano Energy* **18**, 154–164 (2015).
- <sup>173</sup>M. H. Park, H. J. Kim, Y. J. Kim, T. Moon, K. D. Kim, and C. S. Hwang, "Thin Hf<sub>x</sub>Zr<sub>1-x</sub>O<sub>2</sub> films: A new lead-free system for electrostatic supercapacitors with large energy storage density and robust thermal stability," *Adv. Energy Mater.* **4**(16), 1400610 (2014).
- <sup>174</sup>S. J. Kim, J. Mohan, J. S. Lee, H. S. Kim, J. Lee, C. D. Young, L. Colombo, S. R. Summerfelt, T. San, and J. Kim, "Stress-induced crystallization of thin Hf<sub>1-x</sub>Zr<sub>x</sub>O<sub>2</sub> films: The origin of enhanced energy density with minimized energy loss for lead-free electrostatic energy storage applications," *ACS Appl. Mater. Interfaces* **11**(5), 5208–5214 (2019).
- <sup>175</sup>M. Pesic, M. Hoffmann, C. Richter, T. Mikolajick, and U. Schroeder, "Nonvolatile random access memory and energy storage based on antiferroelectric like hysteresis in ZrO<sub>2</sub>," *Adv. Funct. Mater.* **26**(41), 7486–7494 (2016).
- <sup>176</sup>F. Ali, D. Zhou, N. Sun, H. W. Ali, A. Abbas, F. Iqbal, F. Dong, and K.-H. Kim, "Fluorite-structured ferroelectric-/antiferroelectric-based electrostatic nanocapacitors for energy storage applications," *ACS Appl. Energy Mater.* **3**(7), 6036–6055 (2020).
- <sup>177</sup>P. D. Lomenzo, C.-C. Chung, C. Zhou, J. L. Jones, and T. Nishida, "Doped Hf<sub>0.5</sub>Zr<sub>0.5</sub>O<sub>2</sub> for high efficiency integrated supercapacitors," *Appl. Phys. Lett.* **110**(23), 232904 (2017).
- <sup>178</sup>B. B. Yang, M. Y. Guo, D. P. Song, X. W. Tang, R. H. Wei, L. Hu, J. Yang, W. H. Song, J. M. Dai, X. J. Lou, X. B. Zhu, and Y. P. Sun, "Energy storage properties in BaTiO<sub>3</sub>-Bi<sub>3.25</sub>La<sub>0.75</sub>Ti<sub>3</sub>O<sub>12</sub> thin films," *Appl. Phys. Lett.* **113**, 183902 (2018).
- <sup>179</sup>J. Chen, Z. Tang, B. Yang, and S. Zhao, "High energy storage performances in lead-free BaBi<sub>3.9</sub>Pr<sub>0.1</sub>Ti<sub>4</sub>O<sub>15</sub> relaxor ferroelectric films," *Appl. Phys. Lett.* **113**(15), 153904 (2018).
- <sup>180</sup>M. G. Kozodaev, A. G. Chernikova, R. R. Khakimov, M. H. Park, A. M. Markeev, and C. S. Hwang, "La-doped Hf<sub>0.5</sub>Zr<sub>0.5</sub>O<sub>2</sub> thin films for high-efficiency electrostatic supercapacitors," *Appl. Phys. Lett.* **113**(12), 123902 (2018).



- <sup>181</sup>C. Mart, T. Kämpfe, S. Zybelle, and W. Weinreich, "Layer thickness scaling and wake-up effect of pyroelectric response in Si-doped  $\text{HfO}_2$ ," *Appl. Phys. Lett.* **112**, 052905 (2018).
- <sup>182</sup>C. Mart, K. Kühnel, T. Kämpfe, S. Zybelle, and W. Weinreich, "Ferroelectric and pyroelectric properties of polycrystalline La-doped  $\text{HfO}_2$  thin films," *Appl. Phys. Lett.* **114**, 102903 (2019).
- <sup>183</sup>S. W. Smith, M. D. Henry, M. T. Brumbach, M. A. Rodriguez, and J. F. Ihlefeld, "Thickness scaling of pyroelectric response in thin ferroelectric  $\text{Hf}_{1-x}\text{Zr}_x\text{O}_2$  films," *Appl. Phys. Lett.* **113**, 182904 (2018).
- <sup>184</sup>S. Jachalke, T. Schenk, M. H. Park, U. Schroeder, T. Mikolajick, H. Stöcker, E. Mehner, and D. C. Meyer, "Pyroelectricity of silicon-doped hafnium oxide thin films," *Appl. Phys. Lett.* **112**, 142901 (2018).
- <sup>185</sup>M. H. Park, M. Hoffmann, and C. S. Hwang, "Pyroelectric and electrocaloric effects and their applications," in *Ferroelectricity in Doped Hafnium Oxide: Materials, Properties and Devices* (Elsevier, 2019), pp. 217–244.
- <sup>186</sup>C.-B. Eom and S. Trolor-McKinstry, "Thin-film piezoelectric MEMS," *MRS Bull.* **37**, 1007 (2012).
- <sup>187</sup>I. Kanno, "Piezoelectric MEMS: Ferroelectric thin films for MEMS applications," *Jpn. J. Appl. Phys.* **57**(4), 040101 (2018).
- <sup>188</sup>P. D. Lomenzo, S. Jachalke, H. Stoecker, E. Mehner, C. Richter, T. Mikolajick, and U. Schroeder, "Universal Curie constant and pyroelectricity in doped ferroelectric  $\text{HfO}_2$  thin films," *Nano Energy* **74**, 104733 (2020).
- <sup>189</sup>C. Mart, M. Czernohorsky, S. Zybelle, T. Kämpfe, and W. Weinreich, "Frequency domain analysis of pyroelectric response in silicon-doped hafnium oxide ( $\text{HfO}_2$ ) thin films," *Appl. Phys. Lett.* **113**, 122901 (2018).
- <sup>190</sup>C. Mart, W. Weinreich, M. Czernohorsky, S. Riedel, S. Zybelle, and K. Kuhnle, "CMOS compatible pyroelectric applications enabled by doped  $\text{HfO}_2$  films on deep-trench structures," in *48th European Solid-State Device Research Conference (ESSDERC)* (IEEE, 2018).
- <sup>191</sup>N. Kurz, Y. Lu, L. Kirste, M. Reusch, A. Žukauskaitė, V. Lebedev, and O. Ambacher, "Temperature dependence of the pyroelectric coefficient of  $\text{AlScN}$  thin films," *Phys. Status Solidi A* **215**, 1700831 (2018).
- <sup>192</sup>S. Bette, S. Fichtner, S. Bröker, L. Nielen, T. Schmitz-Kempen, B. Wagner, C. Van Buggenhout, S. Tiedke, and S. Tappertzhofen, "Temperature dependence of the pyroelectric coefficient of  $\text{AlScN}$  thin films," *Thin Solid Films* **692**, 137623 (2019).
- <sup>193</sup>C. C. W. Ruppel, "Acoustic wave filter technology—A review," *IEEE Trans. Ultrason. Ferroelectr. Freq. Control* **64**(9), 1390–1400 (2017).
- <sup>194</sup>A. H. Olsson, Z. Tang, and M. D'Agati, "Doping of aluminum nitride and the impact on thin film piezoelectric and ferroelectric device performance," in *IEEE Custom Integrated Circuits Conference (CICC)* (IEEE, 2020), pp. 1–6.
- <sup>195</sup>S. Rassay, F. Hakim, M. Ramezani, and R. Tabrizian, "Acoustically coupled wideband RF filters with bandwidth reconfigurability using ferroelectric aluminum scandium nitride film," in *IEEE 33rd International Conference on Micro Electro Mechanical Systems (MEMS)* (IEEE, 2020), pp. 1254–1257.
- <sup>196</sup>Y. Lu, M. Reusch, N. Kurz, A. Ding, T. Christoph, M. Prescher, L. Kirste, O. Ambacher, and A. Žukauskaitė, "Elastic modulus and coefficient of thermal expansion of piezoelectric  $\text{Al}_{1-x}\text{Sc}_x\text{N}$  (up to  $x = 0.41$ ) thin films," *APL Mater.* **6**, 076105 (2018).
- <sup>197</sup>S. Kirbach, K. Kuhnle, and W. Weinreich, "Piezoelectric hafnium oxide thin films for energy-harvesting," in *IEEE 18th International Conference on Nanotechnology (IEEE-NANO)* (IEEE, 2018), pp. 1–4.
- <sup>198</sup>S. Starschich, T. Schenk, U. Schroeder, and U. Boettger, "Ferroelectric and piezoelectric properties of  $\text{Hf}_{1-x}\text{Zr}_x\text{O}_2$  and pure  $\text{ZrO}_2$  films," *Appl. Phys. Lett.* **110**, 182905 (2017).
- <sup>199</sup>S. Starschich and U. Böttger, "Doped  $\text{ZrO}_2$  for future lead free piezoelectric devices," *J. Appl. Phys.* **123**, 044101 (2018).
- <sup>200</sup>M. Ghatge, G. Walters, T. Nishida, and R. Tabrizian, "A 30-nm thick integrated hafnium zirconium oxide nano-electro-mechanical membrane resonator," *Appl. Phys. Lett.* **116**, 043501 (2020).
- <sup>201</sup>M. Ghatge, G. Walters, T. Nishida, and R. Tabrizian, "An ultrathin integrated nanoelectromechanical transducer based on hafnium zirconium oxide," *Nat. Electron.* **2**, 506–512 (2019).
- <sup>202</sup>M. Ghatge, G. Walters, T. Nishida, and R. R. Tabrizian, "High-Q UHF and SHF bulk acoustic wave resonators with ten-nanometer  $\text{Hf}_{0.5}\text{Zr}_{0.5}\text{O}_2$  ferroelectric transducer," in *20th International Conference on Solid-State Sensors, Actuators and Microsystems & Eurosensors XXXIII* (American Elements, 2019), pp. 446–449.
- <sup>203</sup>T. Mimura, T. Shimizu, and H. Funakubo, "Ferroelectricity in  $\text{YO}_{1.5}\text{-HfO}_2$  films around 1  $\mu\text{m}$  in thickness," *Appl. Phys. Lett.* **115**, 032901 (2019).
- <sup>204</sup>T. Schenk, N. Godard, A. Mahjoub, S. Girod, A. Matavz, V. Bobnar, E. Defay, and S. Glinsek, "Toward thick piezoelectric  $\text{HfO}_2$ -based films," *Physica Status Solidi RRL* **14**, 1900626 (2020).
- <sup>205</sup>K. R. Udayakumar *et al.*, "Manufacturable high-density 8 mbit one transistor-one capacitor embedded ferroelectric random access memory," *Jpn. J. Appl. Phys.* **47**, 2710 (2008).
- <sup>206</sup>M. Pestic, S. Knebel, M. Hoffmann, C. Richter, T. Mikolajick, and U. Schroeder, "How to make DRAM non-volatile? Anti-ferroelectrics: A new paradigm for universal memories," in *IEEE International Electron Devices Meeting (IEDM)* (IEEE, 2016), pp. 11.6. 1–11.6. 4.
- <sup>207</sup>M. Pešić, U. Schroeder, S. Slesazeck, and T. Mikolajick, "Comparative study of reliability of ferroelectric and anti-ferroelectric memories," *IEEE Trans. Device Mater. Reliab.* **18**(2), 154–162 (2018).
- <sup>208</sup>M. Pešić, T. Li, V. D. Lecce, M. Hoffmann, M. Materano, C. Richter, B. Max, S. Slesazeck, U. Schroeder, L. Larcher, and T. Mikolajick, "Built-in bias generation in anti-ferroelectric stacks: Methods and device applications," *IEEE J. Electron Devices Soc.* **6**, 1019–1025 (2018).
- <sup>209</sup>P. Buragohain, A. Erickson, P. Kariuki, T. Mittmann, C. Richter, P. D. Lomenzo, H. Lu, T. Schenk, T. Mikolajick, U. Schroeder, and A. Gruverman, "Fluid imprint and inertial switching in ferroelectric  $\text{La:HfO}_2$  capacitors," *ACS Appl. Mater. Interfaces* **11**(38), 35115–35121 (2019).
- <sup>210</sup>H. Mulaosmanovic, E. T. Breyer, T. Mikolajick, and S. Slesazeck, "Reconfigurable frequency multiplication with a ferroelectric transistor," *Nat. Electron.* **3**, 391–397 (2020).
- <sup>211</sup>O. Auciello, "A critical comparative review of PZT and SBT-based science and technology for non-volatile ferroelectric memories," *Integ. Ferroelectr.* **15**, 1–4 (1997).
- <sup>212</sup>J. F. Scott, *Ferroelectric Memories* (Springer, Berlin, 2000).
- <sup>213</sup>J. F. Scott and C. A. Paz de Araujo, "Ferroelectric memories," *Science* **246**(1936), 1400–1405 (1989).
- <sup>214</sup>S. Beyer, "Embedded FeFETs as a low power and non-volatile beyond-von-Neumann memory solution," in *Nonvolatile Memory Technology Symposium (NVMTS)* (IEEE, 2018).
- <sup>215</sup>E. Breyer, H. Mulaosmanovic, T. Mikolajick, and S. Slesazeck, "Ultra-dense co-integration of FeFETs and n-Fets: Enabling very-fine grained logic-in-memory," in *European Solid-State Device Research Conference (ESSDERC)* (IEEE, 2019).